REVIEW

Local curvatures and its measurements of an optical surface or a wavefront: a review

José Hernández-Delgado,[a,*] **Zacarías Malacara-Hernández**,[a] **Daniel Malacara-Doblado**,[a] **Benito Vázquez-Dorrío**,[b] **and Daniel Malacara-Hernández**[a]

[a]Centro de Investigaciones en Óptica, A.C., Optical Engineering, Lomas del Campestre, León, Gto., México

[b]Universidad de Vigo, Vigo, Spain

Abstract. The mathematical tools to calculate surface and wavefront local curvatures have been growing in importance because, when studying and evaluating some optical systems, the local curvature becomes extremely important. Many practical methods have been created to measure the wavefront shape and local curvatures as well as many mathematical tools to describe them. These methods are very useful in ophthalmology mainly for corneal evaluation, but the methods are now being used in other fields of optical metrology, especially in optical testing, interferometric wavefront description, and others. In some instruments and optical devices, mainly ophthalmic and optometric instruments, the local curvatures distribution over the pupil of an optical system is more important than the wavefront topography. A typical example is a human eye, in which corneal topographers, eye aberrometers, and several other instruments are used to measure the local curvatures. In particular, the main aspects of the curvature calculation at a given point for different slopes in any direction are introduced. The principal curvatures, mean, Gaussian, cylindrical, tangential, and sagittal curvatures are described. In the second part of this review, we describe the main methods and devices for wavefront sensing, measuring elevations, slopes, or curvatures. We conclude with a description of some methods to measure and calculate local curvatures from wavefront sensors by measuring the wavefront elevations, the transverse aberrations (slopes), or directly the curvatures. [DOI: 10.1117/1.OE.61.5.050901]

Keywords: principal curvature; mean curvature; Gaussian curvature; wavefront sensor; corneal imaging; color-map; optical surfaces.

Paper 20211099V received Sep. 29, 2021; accepted for publication Apr. 22, 2022; published online May 23, 2022; corrected Aug. 10, 2022.

1 Introduction

When evaluating most optical systems or surfaces, the wavefront or surface topography becomes extremely important. Typically, it is represented by a topographic map that can be obtained mostly by optical interferometric methods, for example, the Twyman–Green interferometer in Fig. 1(a), representing an astigmatic (sphero-cylindrical deformation) which is a topographic map with equal elevation deformation, where each line represents the geometrical locus of points of equal elevation or separation from its reference sphere. The difference in elevation between two consecutive fringes is one wavelength. Figure 1(b) shows a representation of an equal wavefront map for the constant deviation points where the different colors represent different values of the elevation.

Intuitively, we know that the local curvature tells us how fast the elevation slope changes at some point. In some optical systems, the local curvature instead of the elevation becomes more important since the value of the curvature is an indication of the local convergence or divergence power of the optical surface or the local degree of convergence or divergence in a wavefront. This will be described later in more detail.

*Address all correspondence to José Hernández-Delgado, josehd@cio.mx

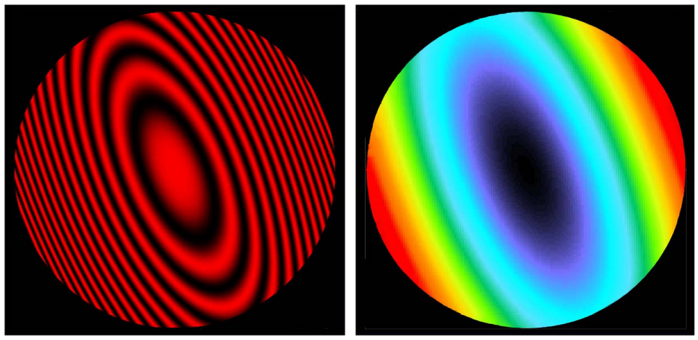

Fig. 1 Maps of equal elevation deformation in a wavefront or surface of an optical system. (a) Twyman–Green interferograms and (b) color-coded map. An advantage of the Twyman–Green interferogram is that it provides more quantitative results than the color-coded map, but a disadvantage is that its elevation has a sign uncertainty that the color-coded map does not have. In the Twyman–Green interferogram, the fringe separation is an indication of the elevation slope.

The geometrical concept of curvature and the mathematical theory of local curvatures are quite old and they are the main subjects of the books about differential geometry. The history of the concept of curvature has been treated recently by many authors with some detail, e.g., by Margalit[1] and Bardini and Gianella.[2] The first attempts to formally define the curvature started many centuries ago, beginning with the Greek writers, following with Johannes Kepler (1571 to 1630) who was the first to define the curvature as the inverse of the local radius of curvature. However, the first successful study comes from Newton,[3] as described by Coolidge.[4] He said that the curvature of a curved line is equal to the curvature of the largest circle that is tangent to the curve on its concave side and that the center of the circle is the center of curvature. The study of curvatures is increasing its importance and has recently become a very important concept in optometry and ophthalmology.[5] It is thus surprising that classical optics books ignore this subject almost completely. Even ophthalmology and optometry books study curvatures at just an introductory level. Mathematicians and specialists in this field are the ones that study this subject in detail and great advances have recently been made. It is the purpose of this article to make a general review of the subject at a level so that opticians, optical engineers, and in general nonspecialists in the field can get an introductory description of the main concepts today in wide use. In this review, we have made all mathematical derivations using elementary concepts of calculus, without the use of differential geometry to make it simpler to understand for nonspecialists. The concept of curvature is so important that has applications in many fields, even as something that can be perceived by just touching the surface[6] and as a tool for neurologic studies.[7]

When evaluating an optical surface, we might be interested in the map of the optical surface or wavefront deformations, frequently called aberrations, as given by an elevation map. A typical example includes the surface of a primary mirror for an astronomical telescope under polishing or figuring. In some other optical surfaces, the important characteristics to be measured are not the optical surface or the wavefront deviation but the local curvatures, as in the case of the human eye corneas. The most commonly evaluated curvatures in optometry and ophthalmology are the sagittal and tangential curvatures and the axis orientation.[5] In most commercial instruments this is done with approximations, frequently with the assumption that the optical surface or wavefront is nearly rotationally symmetric. More general and precise evaluation methods were not found to be described in any general optics, ophthalmology, or optometry books, perhaps with the only exception of the book by Stavroudis.[8] Surprisingly, to our knowledge, this information was absent even in differential geometry books.

The subject of surface topography and shape, of surfaces studied in differential geometry books, among them, by Stoker,[9] Lipschutz,[10] Bronshtein and Semendyayev,[11] Kepr,[12] Gray et al.,[13] and Krauthammer and Ventsel[14] is quite important and useful in many fields, mainly in ophthalmic and optometric optics and in geology.[15] Typically, in these books, the first fundamental and the second fundamental forms are developed, leading to expressions for the principal curvatures but not for the sagittal and tangential curvatures. In optics, these concepts are

useful for the study of many properties of the optical surfaces and wavefronts. The basic intrinsic properties of a surface are described by the fundamental forms of surfaces, which are the subject of differential geometry books. Their results can be applied to study the sagittal and tangential curvatures, but frequently some other methods are used.[16]

2 Curvatures in a Plane Curve

To fully describe the concept of local curvature in a surface, let us first begin by considering a one-dimensional function $f(x)$ represented in a plane, as in Fig. 2, where three circles are drawn close to the curve.

The first circle at the left, in Fig. 2 is intersected by the curve at two points. The second circle touches the curve at only one point, where the first derivative (slope) at this point is the same both at the curve and at the circle. At a given point in the curve, we can trace an infinite number of tangent circles of different sizes, on any side of the curve. The third circle touches the curve in a small region, where both, the first and the second derivatives are the same at the center of the region where they touch each other. At a given point in the curve, we can trace only one of these circles. Then, we say that the circle and the curve are osculating (from Latin: osculum = kiss). The curve at this small region has the same radius of curvature as the osculating circle. The unit normal vector is a vector passing through the point in the curve being considered and pointing to the center of curvature of the osculating circle. The curvature is defined by the inverse of the radius of curvature r. More formally, we may say that for a small length along with the curve ds, the curvature is given by how fast the slope is changing at the point **P** in Fig. 2, then, as defined probably for the first time by Kästner,[17] the curvature along the x-direction c_x at the point **P** would then be expressed as

$$c_x = \frac{\mathrm{d}\alpha_x}{\mathrm{d}s}, \tag{1}$$

where ds is the small length traveled along the curve and dα is the change in the slope of the curve along the x axis. On the other hand, the slope at the same point **P** is given by the derivative of $f(x)$ respect to x

$$\frac{\mathrm{d}f(x)}{\mathrm{d}x} = \tan\,\alpha_x. \tag{2}$$

The second derivative of the function $f(x)$ with respect to x is equal to the curvature only if the slope at that point is zero. Otherwise, the curvature can be found by writing the second derivative at any point where the first derivative (slope angle equal to α_x) is not zero, as follows:

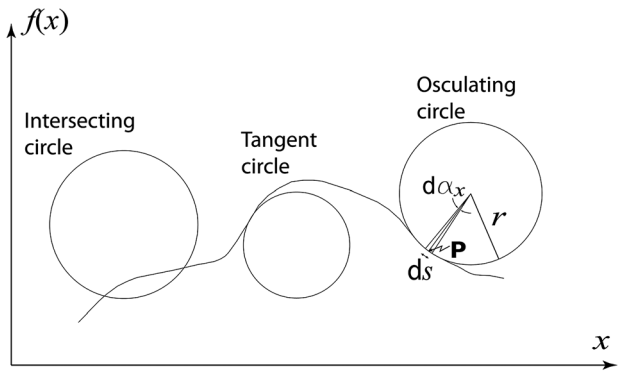

Fig. 2 Three circles near a curve. The first circle is intersected by the curve at two points and the second circle is tangent to the curve at one point. There are many possible tangent circles of any size, at any point. The third circle is osculating to the curve at the point **P**. At a given point in the curve, we can trace only one osculating circle.

$$\frac{\mathrm{d}^2 f(x)}{\mathrm{d}x^2} = \frac{d\,\tan\,\alpha_x}{dx} = \sec^2\alpha_x \frac{d\alpha_x}{dx} = \frac{1}{\cos^2\alpha_x}\frac{d\alpha_x}{ds}\frac{ds}{dx} = \frac{1}{\cos^3\alpha_x} c_x. \tag{3}$$

Hence, the curvature, measured along a curve contained in a flat surface, is given as

$$c_x = \frac{\mathrm{d}^2 f(x)}{\mathrm{d}x^2}\cos^3\alpha_x, \tag{4}$$

which, by writing cos α_x in terms of the tan α_x, which is the first derivative of $f(x)$ respect to x can be written as

$$c_x = \frac{\frac{\mathrm{d}^2 f(x)}{\mathrm{d}x^2}}{\left(1+\left(\frac{\mathrm{d}f(x)}{\mathrm{d}x}\right)^2\right)^{3/2}}. \tag{5}$$

This result was found with a different notation by Bernoulli[18] and more formally some years later by Newton.[3] This curvature is a function of both, the first and the second derivative. If the first derivative is zero, the curvature in the x-direction is just the second derivative of $f(x)$. Thus, we have found expressions to obtain the curvature at a point along a curve $f(x)$ contained in a plane, and the normal to this curve is contained in the same plane.

This result can also be applied to find the exact value of the local curvature over a curve on a surface $f(x,y)$ in the direction of maximum slope (gradient), where the slope in the perpendicular direction is zero. In the next section, we will describe how to find the local curvature along a curve on the surface $f(x,y)$ in the direction of no slope, perpendicularly to the direction of maximum slope.

3 Local Curvatures in a Direction Perpendicular to its Maximum Slope

The concept of curvature was extended by Euler,[19] Bernoulli's doctoral student, to three dimensions. In a more general case we have a surface $f(x,y)$, and a curve on this surface, this expression is strictly valid if the points $\mathbf{P}(x,y)$ where the curvature is to be evaluated has a slope along some direction of the curve but not in the perpendicular direction. We will study the local curvatures over an open surface $f(x,y)$, so that given any point $\mathbf{P}$ with coordinates (x,y) there is only one possible value of the function $f(x,y)$ describing the surface. Let us start by defining some important concepts. A normal plane at a point in a surface is any plane containing the normal to the surface at that point. The intersection of a normal plane with the surface is a curve called a normal section and the curvature of this curve at that point is the normal curvature.

At any point on the surface, we can place a plane tangent at that point. This plane is not necessarily horizontal, which in the general case has a tilt. At the point of tangency on this surface, there is a different slope for different directions, which is equal to the first derivative in the given direction. Thus, at this point, there are two mutually perpendicular directions, one with a zero slope and one with a maximum slope (gradient). It should be pointed out that these zero and maximum slope directions are not necessarily the same as the maximum and minimum curvatures, which are also called the principal curvatures. However, it is interesting to notice two particular cases: (a) If the surface has rotational symmetry, at any off-axis point, the principal curvatures are one in the direction of maximum slope (gradient) and one in the direction of zero slope. In these surfaces, these are the radial and the angular directions. (b) A second interesting case is a surface with symmetry about a straight line in the x–y plane, e.g., a horizontal cylinder. In this case, the principal curvatures are also one in the direction of maximum slope (gradient) and one in the direction of no slope.

The local curvatures at the point in the surface being considered can be easily calculated in these two special directions, i.e., the direction of maximum slope and the direction of zero slope. For the direction of the maximum slope, there is no slope in the perpendicular direction, and hence the theory in Sec. 2 and the result in Eq. (5) can be applied if the x-direction is selected in the direction of maximum slope. Next, we will calculate the local curvature in the direction of zero slope.

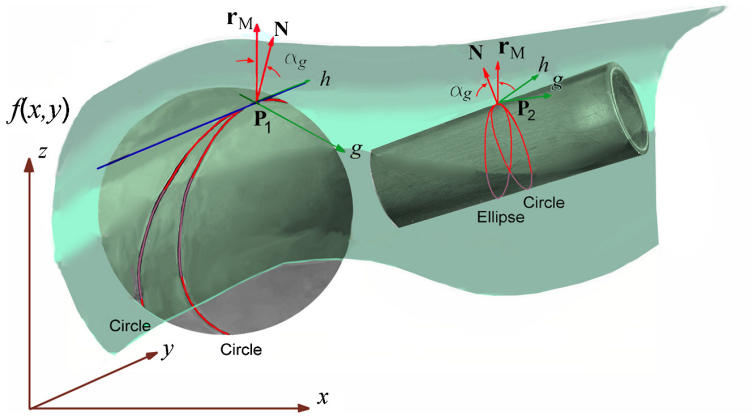

Fig. 3 A surface $f(x, y)$ with an osculating sphere at the point $\mathbf{P}_1$ and an osculating cylinder at the point $\mathbf{P}_2$. The curvature at the two points $\mathbf{P}_1$ and $\mathbf{P}_2$, along the direction of h with no slope is to be measured and the maximum slope is in the direction of g.

Figure 3 illustrates a single-valued function $f(x, y)$, describing a surface on top of a sphere and a cylinder. Let us assume that on this surface we can find two points $\mathbf{P}_1$ and $\mathbf{P}_2$, with the following characteristics. At the point $\mathbf{P}_1$, the local curvatures on this point in the surface $f(x, y)$ are the same in all directions and thus, we can place an osculating sphere at this point. At the point $\mathbf{P}_2$ in the surface $f(x, y)$ the curvature along the x coordinate is zero, hence the axis of the cylinder is contained in a plane perpendicular to the y axis. Thus, we can place an osculating cylinder located at this point $\mathbf{P}_2$. The unit normal vectors $\mathbf{N}$ are at the points where the local curvatures are to be measured. The unit vectors $\mathbf{r}_M$, also at the points $\mathbf{P}_1$ and $\mathbf{P}_2$, are parallel to the z-axis. Thus, the angle between these two vectors $\mathbf{N}$ and $\mathbf{r}_M$ is equal to the angle α_g formed by the maximum slope (gradient) on the surface.

With a simple geometrical analysis, it is relatively simple to show that in general, for the osculating sphere as well as for the osculating cylinder, the curvature in the direction of no slope, which is the perpendicular direction of maximum slope (called here direction h), at a point located along a curve in the plane containing the normal to the surface would be given by the second derivative in this direction, multiplied by cos α_g. Thus, if the slope along the curve in the direction h is zero, but different from zero in the perpendicular direction g, the curvature c_h is

$$c_h = \frac{\partial^2 f}{\partial h^2} \cos \alpha_g. \tag{6}$$

This result is known as the theorem of Meusnier (Truesdell),[20] to honor a mathematical genius that died just before his 39th birthday in Napoleon's army in 1793, after writing his monumental work in differential geometry. Writing cos α_g in terms of tan α_g, which is the first derivative of f respect to g

$$c_h = \frac{\frac{\partial^2 f}{\partial h^2}}{\left(1 + \left(\frac{\partial f}{\partial g}\right)^2\right)^{1/2}}. \tag{7}$$

In conclusion, we can find the exact local curvatures values in the directions of maximum slope and of no slope, using Eqs. (5) and (7), respectively.

4 Curvatures in Different Directions at a Point on a Surface

We have calculated the local curvature at a point in a surface, in two particular mutually perpendicular directions, the direction of maximum slope and the direction of no slope. In any other direction the problem is mathematically more complicated, but the problem has been solved by differential geometry methods, by the development of the first fundamental and the

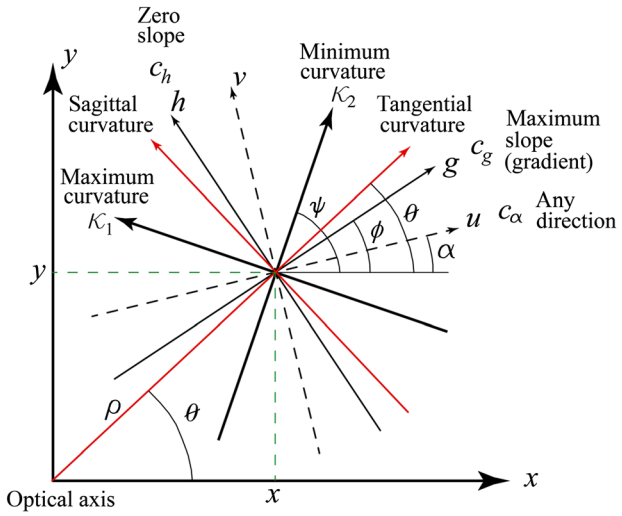

Fig. 4 Different orientations for the zero slope, maximum slope (gradient), the sagittal curvature, the tangential curvature, and the minimum curvature and the maximum curvature (principal curvatures) at a point in a surface.

second fundamental form of surfaces. However, the expressions for c_x and c_h [Eqs. (5) and (7)] are enough to obtain a highly accurate and intuitive method for calculating and understanding the local curvatures as described below.

Let us consider a point in a surface $f(x, y)$ and an infinite number of possible directions for the curvature, passing through a point, as illustrated in Fig. 4.

For this point in this surface, the slopes in the x and y directions are given as

$$\frac{\partial f(x,y)}{\partial x} \quad \text{and} \quad \frac{\partial f(x,y)}{\partial y}. \tag{8}$$

The gradient of the function $f(x, y)$ is a vector in the direction of maximum slope, in the direction of the gradient g, as illustrated in Fig. 4, whose magnitude is given as

$$|\nabla f(x,y)| = \frac{\partial f(x,y)}{\partial g} = \left[\left(\frac{\partial f(x,y)}{\partial x}\right)^2 + \left(\frac{\partial f(x,y)}{\partial y}\right)^2\right]^{1/2}, \tag{9}$$

and the angle with respect to the x axis for the direction of the gradient g is given as

$$\tan\phi = \frac{\left(\frac{\partial f(x,y)}{\partial y}\right)}{\left(\frac{\partial f(x,y)}{\partial x}\right)}. \tag{10}$$

Sometimes, it is necessary to find the values of $\cos 2\phi$ and $\sin 2\phi$, for the gradient direction, which can be shown as

$$\cos 2\phi = \frac{\left(\frac{\partial f}{\partial x}\right)^2 - \left(\frac{\partial f}{\partial y}\right)^2}{\left(\frac{\partial f}{\partial x}\right)^2 + \left(\frac{\partial f}{\partial y}\right)^2}; \quad \sin 2\phi = 2\frac{\left(\frac{\partial f}{\partial x}\right)\left(\frac{\partial f}{\partial y}\right)}{\left(\frac{\partial f}{\partial x}\right)^2 + \left(\frac{\partial f}{\partial y}\right)^2}. \tag{11}$$

The local curvature measured at a point over a surface $f(x, y)$, along the direction of the gradient with the maximum surface slope $\tan\beta_g$ will be represented by c_g and it is given as

$$c_g = \frac{\partial^2 f(x,y)}{\partial g^2}\cos^3\beta_g. \tag{12}$$

The first derivative of $f(x, y)$ with respect to g is

$$\tan \beta_g = \frac{\partial f(x,y)}{\partial g}. \tag{13}$$

Then, writing $\cos \beta_g$ in terms of the $\tan \beta_g$, we obtain

$$c_g = \frac{\frac{\partial^2 f(x,y)}{\partial g^2}}{\left(1 + \left(\frac{\partial f(x,y)}{\partial g}\right)^2\right)^{3/2}}. \tag{14}$$

Thus, formally probing the use of Eq. (5) to find the local curvature along the gradient.

5 Curvatures in a Surface $f(x,y)$ in Any Direction α

Now, to calculate the local curvatures at any point in any desired direction α (see Figs. 4 and 5) we need to know the first and second derivatives at the desired location. Let us assume that we need to calculate the first and second derivatives at the point (x, y) but in the direction α of the rotated coordinates u and v, as illustrated in Fig. 5.

The function representing the surface is $f(x, y)$. The first derivative with respect to the coordinate u, in the α direction as

$$\frac{\partial f(x,y)}{\partial u} = \frac{\partial f}{\partial x} \cos \alpha + \frac{\partial f}{\partial y} \sin \alpha, \tag{15}$$

and the first derivative with respect to the coordinate v in the $\alpha + 90$ deg direction as

$$\frac{\partial f(x,y)}{\partial v} = -\frac{\partial f}{\partial x} \sin \alpha + \frac{\partial f}{\partial y} \cos \alpha. \tag{16}$$

The second derivative of $f(x, y)$ with respect to the coordinate u is given as

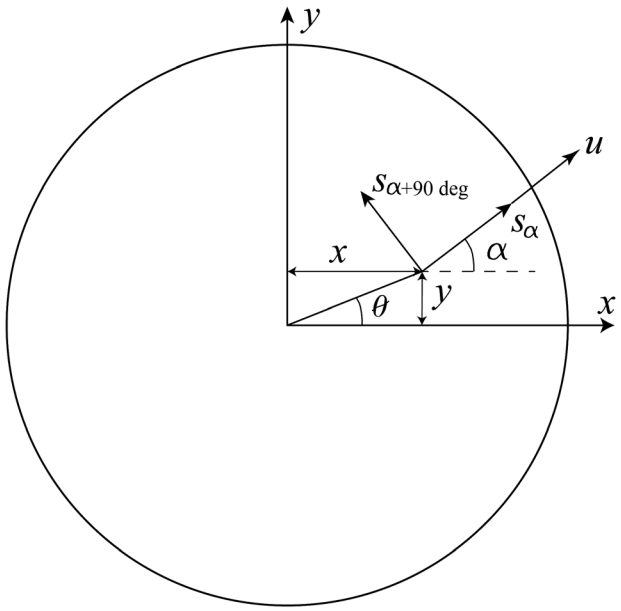

Fig. 5 Translation and rotation of coordinates to evaluate the local curvatures at the point (x, y) along the rotated axis u in the direction α.

$$\begin{aligned}\frac{\partial^2 f(x,y)}{\partial u^2} &= \frac{\partial}{\partial u}\left(\cos\,\alpha\frac{\partial f}{\partial x}+\sin\,\alpha\frac{\partial f}{\partial y}\right)\\ &= \left(\cos\,\alpha\frac{\partial}{\partial x}+\sin\,\alpha\frac{\partial}{\partial y}\right)\left(\cos\,\alpha\frac{\partial f}{\partial x}+\sin\,\alpha\frac{\partial f}{\partial y}\right)\\ &= \frac{\partial^2 f}{\partial x^2}\cos^2\alpha+\frac{\partial^2 f}{\partial y^2}\sin^2\alpha+2\frac{\partial^2 f}{\partial x\partial y}\,\sin\,\alpha\,\cos\,\alpha\\ &= \frac{1}{2}\left(\frac{\partial^2 f}{\partial x^2}+\frac{\partial^2 f}{\partial y^2}\right)+\frac{1}{2}\left(\frac{\partial^2 f}{\partial x^2}-\frac{\partial^2 f}{\partial y^2}\right)\cos\,2\alpha+\frac{\partial^2 f}{\partial x\partial y}\,\sin\,2\alpha. \end{aligned} \tag{17}$$

This second derivative along the u axis, in the direction given by this expression is equal to the curvature c_θ only when the slopes at the point in the surface where this curvature is to be evaluated are zero.

Now, let us now assume that this surface normal is not perpendicular to the x–y plane. We assume there is a slope $\tan\beta_u$ along the curve where the curvature is measured, given by the first derivative with respect to the coordinate u, in the direction as

$$\tan\,\beta_u = \frac{\partial f}{\partial u} = \frac{\partial f}{\partial x}\,\cos\,\alpha+\frac{\partial f}{\partial y}\,\sin\,\alpha. \tag{18}$$

If besides this inclination of the surface normal in the direction of the measurement, there is also a slope of the surface or inclination α_v of the surface normal in the perpendicular direction, we might intuitively try to generalize our two curvature expressions [Eqs. (7) and (14)] by writing

$$c_\alpha = \frac{\partial^2 f(x,y)}{\partial u^2}\cos^3\beta_u\,\cos\,\beta_v, \tag{19}$$

where the directions u and v are mutually perpendicular. Then, by writing the $\cos\,\beta_u$ and $\cos\,\beta_v$ in terms of the slopes we can find

$$c_\alpha = \frac{\frac{1}{2}\left(\frac{\partial^2 f}{\partial x^2}+\frac{\partial^2 f}{\partial y^2}\right)+\frac{1}{2}\left(\frac{\partial^2 f}{\partial x^2}-\frac{\partial^2 f}{\partial y^2}\right)\cos\,2\alpha+\frac{\partial^2 f}{\partial x\partial y}\,\sin\,2\alpha}{\left[1+\left(\frac{\partial f}{\partial x}\,\cos\,\alpha+\frac{\partial f}{\partial y}\,\sin\,\alpha\right)^2\right]^{3/2}\left[1+\left(\frac{\partial f}{\partial x}\,\sin\,\alpha-\frac{\partial f}{\partial y}\,\cos\,\alpha\right)^2\right]^{1/2}}. \tag{20}$$

This expression was derived here in an intuitive manner, and it is exact only in the directions of the gradient $\alpha=\phi$ (and $\alpha=\phi+180$ deg) and perpendicular to the gradient $\alpha=\phi+90$ deg (and $\alpha=\phi+270$ deg). Although it is only approximate, it is highly accurate in all other directions and exact if its slopes are zero.

The exact formula derived in a rigorous manner from the fundamental forms of the differential geometry. From the book by Stoker[9] after converting to Cartesian coordinates by a Monge parametrization, the exact curvature expression is quite similar, as follows:

$$c_\alpha = \frac{\frac{1}{2}\left(\frac{\partial^2 f}{\partial x^2}+\frac{\partial^2 f}{\partial y^2}\right)+\frac{1}{2}\left(\frac{\partial^2 f}{\partial x^2}-\frac{\partial^2 f}{\partial y^2}\right)\cos\,2\alpha+\frac{\partial^2 f}{\partial x\partial y}\,\sin\,2\alpha}{\left[1+\left(\frac{\partial f}{\partial x}\,\cos\,\alpha+\frac{\partial f}{\partial y}\,\sin\,\alpha\right)^2\right)\left(1+\left(\frac{\partial f}{\partial x}\right)^2+\left(\frac{\partial f}{\partial y}\right)^2\right]^{1/2}}. \tag{21}$$

Its derivation is made with curvilinear coordinates, obtaining the first and second fundamental forms of surfaces in three-dimensional space. The Monge parametrization can be made when the surface does not deviate much from a plane, but it deviates enough to make the first derivatives sufficiently large to make the denominator factors in this expression significant. Observing this expression, we may notice that the whole denominator becomes equal to one if the first derivatives are extremely small or zero. Then, the curvature is just the numerator, which is equal to the second derivative in the direction of the measured curvature.

If the expression is converted from Cartesian to polar coordinates, the exact expression for the local curvatures at the point (ρ,θ) becomes

$$c_\alpha = \frac{\frac{1}{2}\left(\frac{\partial^2 f}{\partial \rho^2} + \frac{1}{\rho}\frac{\partial f}{\partial \rho} + \frac{1}{\rho^2}\frac{\partial^2 f}{\partial \theta^2}\right) + \frac{1}{2}\left(\frac{\partial^2 f}{\partial \rho^2} - \frac{1}{\rho}\frac{\partial f}{\partial \rho} - \frac{1}{\rho^2}\frac{\partial^2 f}{\partial \theta^2}\right)\cos\,2(\theta-\alpha) - \frac{1}{\rho}\left(\frac{\partial^2 f}{\partial \rho \partial \theta} - \frac{1}{\rho}\frac{\partial f}{\partial \theta}\right)\sin\,2(\theta-\alpha)}{\left(1 + \left(\frac{\partial f}{\partial \rho}\,\cos(\theta-\alpha) - \frac{1}{\rho}\frac{\partial f}{\partial \theta}\,\sin(\theta-\alpha)\right)^2\right)\left(1 + \left(\frac{\partial f}{\partial \rho}\right)^2 + \frac{1}{\rho^2}\left(\frac{\partial f}{\partial \theta}\right)^2\right)^{1/2}}. \tag{22}$$

Observing Eq. (21), if we define an angle ψ as

$$B\,\cos\,2\psi = \frac{1}{2}\left(\frac{\partial^2 f}{\partial x^2} + \frac{\partial^2 f}{\partial y^2}\right) \quad \text{and} \quad B\,\sin\,2\psi = \left(\frac{\partial^2 f}{\partial x \partial y}\right)^2. \tag{23}$$

Calculating B from these expressions and after some algebraic manipulation, this Eq. (21) can be transformed into

$$c_\alpha = \frac{\frac{1}{2}\left(\frac{\partial^2 f}{\partial x^2} + \frac{\partial^2 f}{\partial y^2}\right) + \left[\frac{1}{4}\left(\frac{\partial^2 f}{\partial x^2} - \frac{\partial^2 f}{\partial y^2}\right)^2 + \left(\frac{\partial^2 f}{\partial x \partial y}\right)^2\right]^{1/2}\cos\,2(\alpha-\psi)}{\left(1 + \left(\frac{\partial f}{\partial x}\,\cos\,\alpha + \frac{\partial f}{\partial y}\,\sin\,\alpha\right)^2\right)\left(1 + \left(\frac{\partial f}{\partial x}\right)^2 + \left(\frac{\partial f}{\partial y}\right)^2\right)^{1/2}}, \tag{24}$$

which is quite similar to the Euler relation described later in Sec. 7 and where ψ is the orientation of the cylindrical axis, given as

$$\tan\,\psi = \frac{2\frac{\partial^2 f}{\partial x \partial y}}{\frac{\partial^2 f}{\partial x^2} - \frac{\partial^2 f}{\partial y^2}}. \tag{25}$$

6 Accuracy of the Approximate Formula to Determine Curvatures in any Direction

The determination of the local curvatures in a wavefront in an optical system is of great importance. It was shown by Kneisly[21] that they can, in principle, be determined by studying the propagation of light beams in an optical system by means of ray tracing. Following our treatment, we have pointed out that the expression 20 provides only an approximate value for the curvatures in directions different from those of the gradient direction and perpendicularly to the gradient.

Exact results can be obtained only using the results from the fundamental forms of surfaces, as studied in differential geometry, in Eqs. (20) or (21). However, the result is quite accurate. An expression for the curvature error can be calculated by taking the difference between the approximate expression obtained here and the exact expression as follows:

$$\begin{aligned}\Delta c_\alpha = &\frac{\frac{1}{2}\left(\frac{\partial^2 f}{\partial x^2} + \frac{\partial^2 f}{\partial y^2}\right) + \frac{1}{2}\left(\frac{\partial^2 f}{\partial x^2} - \frac{\partial^2 f}{\partial y^2}\right)\cos\,2\alpha + \frac{\partial^2 f}{\partial x \partial y}\,\sin\,2\alpha}{\left[1 + \left(\frac{\partial f}{\partial x}\cos\,\alpha + \frac{\partial f}{\partial y}\sin\,\alpha\right)^2\right]^{3/2}\left[1 + \left(\frac{\partial f}{\partial x}\,\sin\,\alpha - \frac{\partial f}{\partial y}\,\cos\,\alpha\right)^2\right]^{1/2}}, \\ &- \frac{\frac{1}{2}\left(\frac{\partial^2 f}{\partial x^2} + \frac{\partial^2 f}{\partial y^2}\right) + \frac{1}{2}\left(\frac{\partial^2 f}{\partial x^2} - \frac{\partial^2 f}{\partial y^2}\right)\cos\,2\alpha + \frac{\partial^2 f}{\partial x \partial y}\,\sin\,2\alpha}{\left(1 + \left(\frac{\partial f}{\partial x}\,\cos\,\alpha + \frac{\partial f}{\partial y}\,\sin\,\alpha\right)^2\right)\left(1 + \left(\frac{\partial f}{\partial x}\right)^2 + \left(\frac{\partial f}{\partial y}\right)^2\right)^{1/2}},\end{aligned} \tag{26}$$

and thus, the error divided by the curvature as

$$\frac{\Delta c_\alpha}{c_\alpha} = \frac{\left(\frac{N}{D_1} - \frac{N}{D_2}\right)}{\left(\frac{N}{D_1}\right)} = \left(\frac{D_2 - D_1}{D_2}\right), \tag{27}$$

where N is the numerator in Eq. (26), D_1 is the first factor of the denominator and D_2 is the second factor. Hence, we may find after some algebraic manipulation, and using Eq. (10) for the orientation of the gradient:

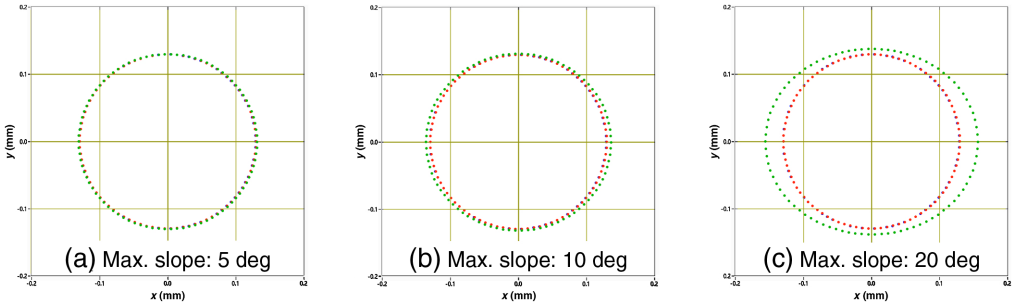

Fig. 6 (a)–(c) Three polar representations of the local curvatures in all directions at three-point in a sphere with different distances from the axis. At these points the gradient or maximum slope is different. Each figure has three different polar plots, one of them, with blue dots, is a perfect circle, calculated with the exact expression for the curvatures (local curvature equal to 0.13 mm^{-1}). Another, with red dots, is calculated with the approximate expression. It is quite close to the circle and touches over the line along the gradient and along a line perpendicular to the gradient. The third polar plot is for the local curvatures with green dots, calculated just with the numerator of the expression for the curvatures. All three polar plots become identical to a circle (zero error) when the maximum slope is zero (at the optical axis).

$$\frac{\Delta c_\alpha}{c_\alpha} = 1 - \left[1 + \frac{\left(\left(\frac{\partial f}{\partial x}\right)^2 + \left(\frac{\partial f}{\partial y}\right)^2\right)^2}{8\left(1 + \left(\frac{\partial f}{\partial x}\right)^2 + \left(\frac{\partial f}{\partial y}\right)^2\right)}(1 - \cos 4(\alpha - \phi))\right]^{1/2}, \tag{28}$$

and using an expression for the magnitude of the gradient

$$\frac{\Delta c_\alpha}{c_\alpha} = 1 - \left[1 + \frac{|\nabla f(x,y)|^4}{8(1 + |\nabla f(x,y)|^2)}(1 - \cos 4(\alpha - \phi))\right]^{1/2}. \tag{29}$$

We can see that the maximum error is a function only of the magnitude of the gradient, that is, of the maximum slope at the point where the curvature is evaluated. If we add this value of Δc_θ to the approximate expression, the small remaining error is compensated, thus obtaining an exact result. As we can observe, the error amplitude depends only on the magnitude of the gradient, or maximum slope of the tangent plane at the point where the curvature is evaluated. We might observe that the error is zero in the directions of maximum and minimum slope (gradient direction) and in the direction of zero slope (perpendicularly to the gradient). The maximum error is ± 45 deg with respect to the gradient direction.

Figure 6 shows three polar representations of the approximate and the exact curvatures in all directions for a point in a spherical surface and a radius of curvature equal to 7.722 mm, the average radius of the human cornea.

7 Euler Curvature Formula

A point in a surface contains an infinite number of normal planes in all possible directions. These normal planes at a point in a surface in most surfaces and points have different values for different directions, except at points with perfectly spherical or flat shapes.

The expression for the curvature in any direction θ can be expressed in the following form, known as the Euler's curvature formula,[12,13] graphically represented by a closed figure frequently resembling an ellipse, but sometimes it is more like a nut.

The Euler formula representing the polar distribution of the curvature for different angular directions is illustrated in Fig. 7, with an axis orientation $\psi = 0$ deg and different values of the ratio of the cylindrical curvature to the spherical curvature.

In any kind of surface, except in a sphere, the curvature at any point is not necessarily constant, but variable with the direction, in a nearly ellipsoidal manner. In other words, a plot of the

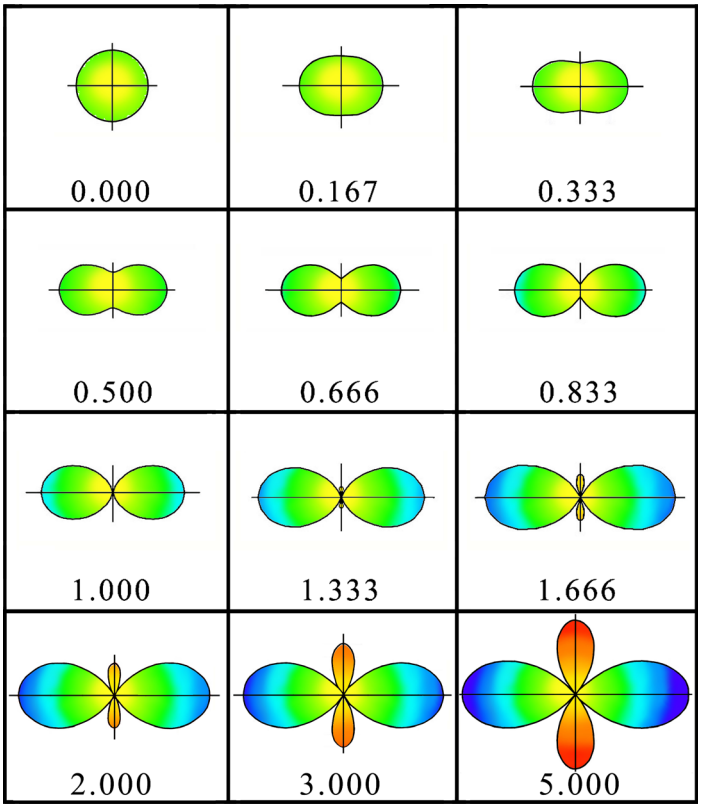

Fig. 7 Polar plots of the Euler formula for an axis orientation ψ equal to 0 deg and different values of the ratio of the cylindrical curvature to the spherical curvature. The color indicates the magnitude of the curvature.

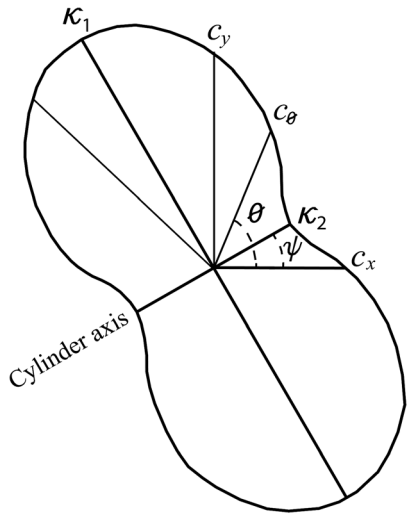

Fig. 8 Variation in the value of the normal curvature cα for all possible directions. The maximum and minimum curvatures, also called principal curvatures κ_1 and κ_2 are orthogonal to each other.

curvature as a function of the angle describes a closed path, as in Fig. 8, with an inclination ψ of the cylinder axis, given by Eq. (24).

There is a maximum value of the curvature κ_1 in one direction and a minimum value κ_2 in an orthogonal direction. These are the two principal curvatures. The principal curvatures are the maximum and minimum local curvatures, which are always perpendicular to each other. If the principal curvatures at a point in an optical surface are κ_1 at an angle $\alpha = \psi \pm \pi$ and κ_2 at an

angle $\alpha = \psi \pm \pi + \pi/2$ the curvature along a direction θ can also be written in terms of the principal curvatures, as illustrated in Fig. 8.

Analytically, this curvature can be represented by the Euler curvature formula which is illustrated in Fig. 9(a) as

$$c_\alpha = \left(\frac{\kappa_1 + \kappa_2}{2}\right) + \left(\frac{\kappa_1 - \kappa_2}{2}\right) \cos\, 2(\alpha - \psi)$$
$$= (c_{\text{sph}})_a + (c_{\text{cyl}})_a \cos\, 2(\alpha - \psi). \tag{30}$$

At the normal plane at an angle ψ the curvature has its maximum value κ_1. In a sphero-cylindrical or toroidal lens the curvature changes in the same manner for planes with different orientations containing the optical axis. If the Euler expression for curvatures is used, κ_1 and κ_2 are the maximum and minimum curvatures, respectively.

The Euler expression for local curvatures can be written in several other different equivalent manners, e.g.

$$c_\alpha = \kappa_2 + (\kappa_1 - \kappa_2)\cos^2(\alpha - \psi)$$
$$= (c_{\text{sph}})_b + (c_{\text{cyl}})_b \cos^2(\alpha - \psi), \tag{31}$$

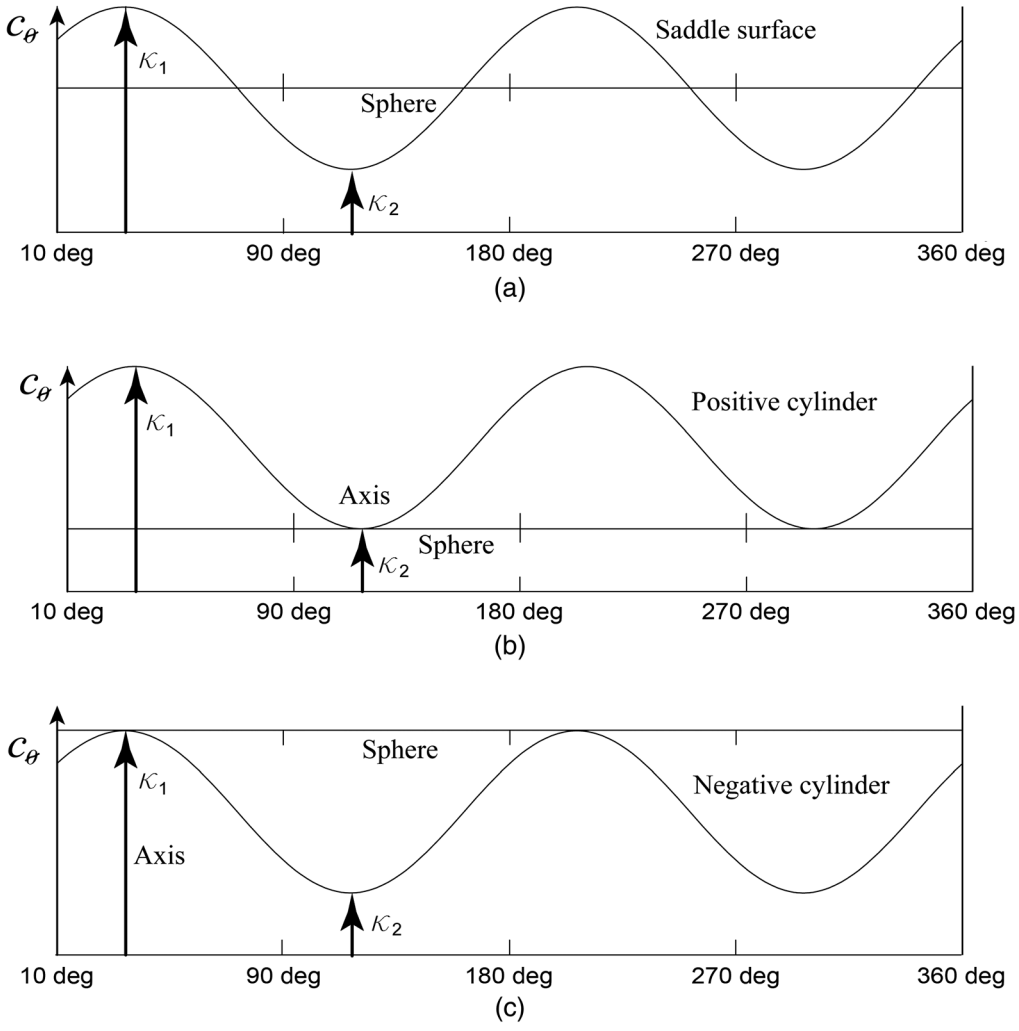

Fig. 9 Curvature variation with the angle at a point in a surface. The total curvature can be expressed as a sum of a spherical and an astigmatic curvature. The spherical component can have: (a) a curvature equal to the average curvature, (b) a curvature equal to its minimum value, and (c) a curvature equal to its maximum value.

as illustrated in Fig. 9(b) and as in Fig. 9(c)

$$c_\alpha = \kappa_1 - (\kappa_1 - \kappa_2)\cos^2(\alpha - \psi \pm 90 \text{ deg}) = (c_{\text{sph}})_c + (c_{\text{cyl}})_c \cos^2(\alpha - \psi \pm 90 \text{ deg}), \tag{32}$$

where c_{sph} is the spherical curvature and c_{cyl} is the cylindrical curvature. Equations (31)[22] and (32) [Figs. 9(b) and 9(c)] are said to be transposed one from the other. A simple method to go from one of them to the other is by means of three simple steps:

1. The new first coefficient (also called the sphere) is obtained by summing the old sphere with the old second coefficient (also called the cylinder). This is the new sphere value.
2. The new cylinder is obtained by changing the sign of the old cylinder.
3. The axis orientation ψ is rotated ± 90 deg.

This can be written as

$$(c_{\text{sph}})_c = (c_{\text{sph}})_b + (c_{\text{cyl}})_b \quad (c_{\text{cyl}})_c = -(c_{\text{cyl}})_b \quad \psi_c = \psi_b + 90 \text{ deg}, \tag{33}$$

or

$$(c_{\text{sph}})_b = (c_{\text{sph}})_c + (c_{\text{cyl}})_c, \quad (c_{\text{cyl}})_b = -(c_{\text{cyl}})_c, \quad \psi_b = \psi_c + 90 \text{ deg}. \tag{34}$$

Another possible representation of the Euler curvature formula is

$$c_\alpha = \kappa_1 \cos^2(\alpha - \psi) + \kappa_2 \sin^2(\alpha - \psi). \tag{35}$$

8 Mean, Gaussian, and Cylindrical Curvatures

Efforts had been made to find parameters that define as simple and as clear as possible the shape of a surface in a small region.[23] Besides the previously described curvatures, in differential geometry, the mean curvature c_{mean} and the Gaussian curvature c_{gauss} have been defined as the arithmetic average and the product, respectively, of the two principal curvatures, as follows:

$$c_{\text{mean}} = \frac{\kappa_1 + \kappa_2}{2} \quad \text{and} \quad c_{\text{gauss}} = \kappa_1 \kappa_2. \tag{36}$$

These two curvatures, mainly the mean curvature, had been used to detect some important shape characteristics in the cornea of the human eye, e.g., the presence of keratoconus, a deformation and thinning near the center, producing a cone-like bulking of the cornea as described by Nasrin et al.,[24] who also made measurements of the curvature in the internal surface of the cornea in a process called pachimetry.

Using Euler [Eq. (31)], we may find the mean curvature as the arithmetic average of the two principal curvatures or in a more general manner as the arithmetic average of any two curvatures in orthogonal directions, as follows:

$$c_{\text{mean}} = \frac{c_\alpha + c_{\alpha+90 \text{ deg}}}{2} = \frac{\kappa_1 + \kappa_2}{2} = \frac{c_g + c_h}{2}. \tag{37}$$

Using here Eq. (21), we can obtain the mean curvature, as follows:

$$c_{\text{mean}} = \frac{\left(\frac{\partial^2 f}{\partial x^2} + \frac{\partial^2 f}{\partial y^2}\right)}{2\left(1 + \left(\frac{\partial f}{\partial x}\cos\alpha + \frac{\partial f}{\partial y}\sin\alpha\right)^2\right)\left(1 + \left(\frac{\partial f}{\partial x}\right)^2 + \left(\frac{\partial f}{\partial y}\right)^2\right)^{1/2}}, \tag{38}$$

which, for surface with symmetry of revolution, becomes

$$c_{\text{mean}} = \left(\frac{\frac{\partial^2 f}{\partial \rho^2} + \frac{1}{\rho}\frac{\partial f}{\partial \rho}\left(1 + \left(\frac{\partial f}{\partial \rho}\right)^2\right)}{2\left[1 + \left(\frac{\partial f}{\partial \rho}\right)^2\right]^{3/2}} \right). \tag{39}$$

If the tangent plane is horizontal, i.e., if the slopes in any direction are zero, the mean curvature can be written as half the Laplacian, as follows:

$$c_{\text{mean}} = \frac{1}{2}\nabla^2 f = \frac{1}{2}\left(\frac{\partial^2 f}{\partial x^2} + \frac{\partial^2 f}{\partial y^2}\right). \tag{40}$$

However, if the slopes (first derivatives) are not zero, this expression is not accurate and may have a significant error.[24]

Individually, these two curvatures hide any information about the difference between the two principal curvatures, frequently called astigmatism, and just specify the arithmetic and the geometric average of the two principal curvatures, representing the curvatures of two intermediate reference spheres, tangent at the point under consideration. The mean curvature is represented by the radius of a circle in Fig. 10.

The Gaussian curvature is the square of the geometric average of the two principal curvatures and has units of $1/\text{mm}^2$ instead of 1/mm as the other curvatures. It is the area of the rectangle in the upper part of Fig. 10. A sphere has a constant curvature over the whole surface. Some other surfaces may have a constant Gaussian curvature over the whole surface, e.g., Fig. 11 illustrates three surfaces with different constant Gaussian curvatures, inside and outside of the surface.

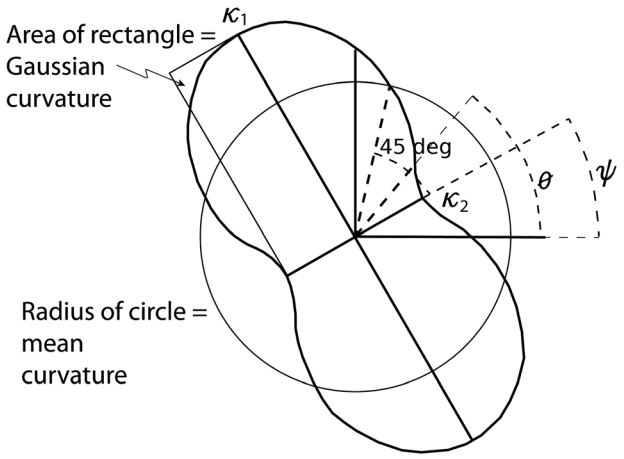

Fig. 10 Polar representation of the Gaussian and mean curvatures.

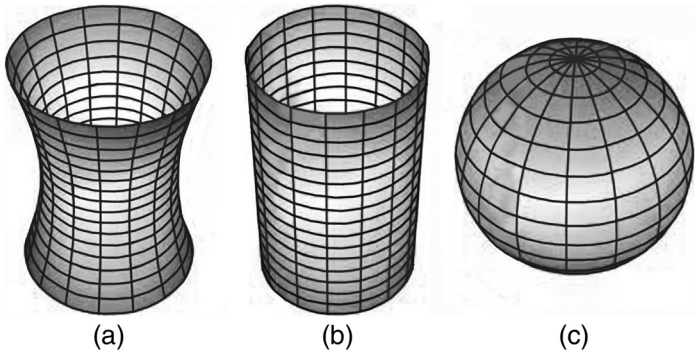

Fig. 11 Three surfaces with different values of the Gaussian curvature. The three surfaces have the same constant value of the Gaussian curvature at all points, inside and outside of the surface. (a) Negative, (b) zero, and (c) positive.

The first surface has negative value, the second one zero values and the third one positive values. The measurement of the Gaussian curvature by optical means has been mathematically studied by Roitman.[25]

If both principal curvatures have the same sign, the Gaussian curvature is positive and that point at the surface is said to be an elliptic point. If both principal curvatures are equal, that point at the surface is said to be an umbilical point and it is locally spherical. The name comes from the Latin *umbilicus*, meaning navel. If the two principal curvatures have different signs, the Gaussian curvature is negative and that point at the surface is said to be a hyperbolic or saddle point. If one of the principal curvatures is zero, the Gaussian curvature is zero and that point at the surface is said to be a parabolic point. This concept of Gaussian curvature has been used in optical design studies.[25,26]

In general, a surface has different values of the mean and the Gaussian curvatures at different points.

The local powers in diopters D_s and D_t are just the curvatures c_s and c_t, multiplied by the index of refraction $n = 1.3375 - 1(n-1)$ as follows:

$$D_s = 0.3375 c_s \quad \text{and} \quad D_t = 0.3375 c_t. \tag{41}$$

It is important to point out that these dioptric powers are valid for a collimated and narrow beam of light entering perpendicularly to the optical surface at the point where the curvatures are considered. If a wide collimated beam of light enters the cornea of the eye, illuminating the whole pupil, the light will not enter perpendicularly to the surface at all points inside the pupil. Dioptric powers with different definitions may appear in this case.[27] For this reason, frequently, these local powers are said to be paraxial approximations.

The cylindrical curvature, from Eqs. (29) and (38), is given as

$$c_{\text{cyl}} = \left(\frac{\kappa_1 - \kappa_2}{2}\right) = \frac{\left[\frac{1}{4}\left(\frac{\partial^2 f}{\partial x^2} - \frac{\partial^2 f}{\partial y^2}\right)^2 + \left(\frac{\partial^2 f}{\partial x \partial y}\right)^2\right]^{1/2}}{\left(1 + \left(\frac{\partial f}{\partial x}\cos\alpha + \frac{\partial f}{\partial y}\sin\alpha\right)^2\right)\left(1 + \left(\frac{\partial f}{\partial x}\right)^2 + \left(\frac{\partial f}{\partial y}\right)^2\right)^{1/2}}. \tag{42}$$

After the mean and the cylindrical local curvatures are calculated with Eqs. (38) and (42), the principal curvatures can easily be obtained.

9 Calculating Astigmatic Parameters with Three Measurements

The curvatures along the gradient and perpendicularly to it do not provide all the information about the curvature variation with normal plane orientation. A third parameter is needed to obtain the Euler equation and thus the curvatures in all directions. This information also allows us to retrieve the cylinder orientation ψ.

In general, to calculate axis orientation, ψ we take a minimum of three measurements of the curvature in three different directions, as in phase-shifting techniques used in optical testing.[23] If we set $\theta_1 = \phi$, $\theta_2 = \phi + 45$ deg, and $\theta_3 = \phi + 90$ deg and two of these three measurements will be the curvatures along the gradient and along the perpendicular to the gradient. The third measurement is at 45 deg between them. Thus, using the Euler equation we have

$$c_g = \left(\frac{\kappa_1 + \kappa_2}{2}\right) + \left(\frac{\kappa_1 - \kappa_2}{2}\right)\cos 2(\phi - \psi), \tag{43}$$

$$c_{45} = \left(\frac{\kappa_1 + \kappa_2}{2}\right) - \left(\frac{\kappa_1 - \kappa_2}{2}\right)\sin 2(\phi - \psi), \tag{44}$$

$$c_h = \left(\frac{\kappa_1 + \kappa_2}{2}\right) - \left(\frac{\kappa_1 - \kappa_2}{2}\right)\cos 2(\phi - \psi). \tag{45}$$

Now, from Eqs. (44) and (45)

$$\tan 2(\phi-\psi)=-\frac{c_{45}-\left(\frac{\kappa_1+\kappa_2}{2}\right)}{c_g-\left(\frac{\kappa_1+\kappa_2}{2}\right)}=\frac{c_g+c_h-2c_{45}}{c_g-c_h}. \tag{46}$$

Then, the cylindrical component (difference between the two principal curvatures), as

$$\left(\frac{\kappa_1-\kappa_2}{2}\right)=\left[c_g-\left(\frac{\kappa_1+\kappa_2}{2}\right)\right][1+\tan^2 2(\phi-\psi)]^{1/2}, \tag{47}$$

but using Eqs. (46) and (47)

$$\left(\frac{\kappa_1-\kappa_2}{2}\right)=\left(\frac{c_g-c_h}{2}\right)\left[1+\left(\frac{c_g+c_h-2c_{45}}{c_g-c_h}\right)^2\right]^{1/2}. \tag{48}$$

The principal curvatures can be obtained from Eqs. (44) and (46)

$$\begin{aligned}\kappa_1&=\frac{(c_g+c_h)}{2}+\frac{(c_g-c_h)}{2}\left[1+\left(\frac{c_g+c_h-2c_{45}}{c_g-c_h}\right)^2\right]^{1/2},\\ \kappa_2&=\frac{(c_g+c_h)}{2}-\frac{(c_g-c_h)}{2}\left[1+\left(\frac{c_g+c_h-2c_{45}}{c_g-c_h}\right)^2\right]^{1/2}.\end{aligned} \tag{49}$$

10 Local Curvatures in Optical Surfaces

In lens design and evaluation programs, the optical surface shape[28] (sagittal distribution) is defined as

$$z(\rho,\theta)=\frac{c\rho^2}{1+[1-(K+1)c^2\rho^2]^{1/2}}+\sum_{j=1}^{4}A_n\rho^{2(n+1)}, \tag{50}$$

where the first term is a conic surface (sphere, ellipsoid, or hyperboloid), K is the conic constant, $\rho^2=x^2+y^2$, c is the vertex curvature of the reference sphere, A_n is the deformation coefficients for rotationally symmetric aspheric surfaces. It is important to point out that the contributions to the sagitta of the aspheric deformations are all in the direction of the optical axis and not perpendicular the reference sphere.

For an optical surface with a circular boundary or a wavefront from an optical system with a circular optical pupil, two curvatures are frequently important. One is in the radial direction, the tangential or radial curvature also called instantaneous curvature. The other curvature in a perpendicular direction, the sagittal or azimuthal curvature c_s, is also called axial curvature by optometrists and ophthalmologists (see Fig. 12).

Using the general expression in polar coordinates, Eq. (22) for local curvatures, the tangential (also called radial or instantaneous) curvatures can be found by setting $\alpha=\theta$, obtaining

$$c_T=\frac{\frac{\partial^2 f}{\partial\rho^2}}{\left(1+\left(\frac{\partial f}{\partial\rho}\right)^2\right)\left(+\left(\frac{\partial f}{\partial\rho}\right)^2+\frac{1}{\rho^2}\left(\frac{\partial f}{\partial\theta}\right)^2\right)^{1/2}}, \tag{51}$$

and using the same general expression, the sagitta (also called axial or azimuthal) can be obtained by setting $\alpha=\theta+90$ deg

$$c_S=\frac{\left(\frac{1}{\rho}\frac{\partial f}{\partial\rho}+\frac{1}{\rho^2}\frac{\partial^2 f}{\partial\theta^2}\right)}{\left(1+\frac{1}{\rho^2}\left(\frac{\partial f}{\partial\theta}\right)^2\right)\left(1+\left(\frac{\partial f}{\partial\rho}\right)^2+\frac{1}{\rho^2}\left(\frac{\partial f}{\partial\theta}\right)^2\right)^{1/2}}. \tag{52}$$

These two expressions are valid for optical surfaces or wavefronts without any aberrations, including those with extreme asymmetries. However, many ophthalmic or optometric surfaces,

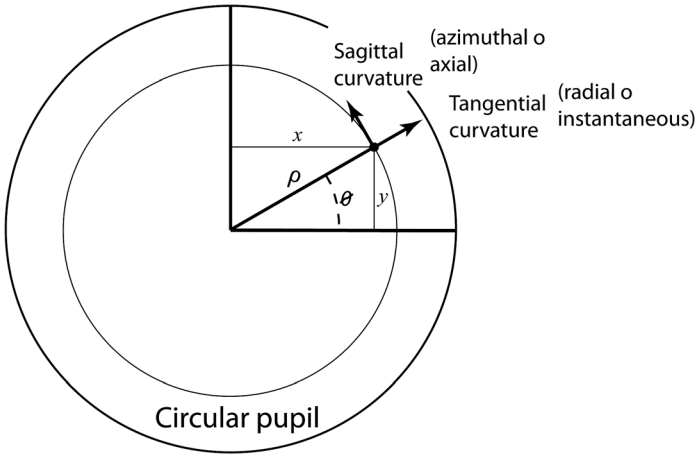

Fig. 12 Tangential or instantaneous and sagittal or axial curvatures in a circular pupil.

e.g., most human eye corneas, are nearly rotational symmetric, if the aberrations are not very large. In this case, the tangential and sagittal expressions for the local curvatures can be simplified by setting the first and second derivatives of f respect to θ equal to zero, as follows:

$$c_T = \frac{\frac{\partial^2 f}{\partial \rho^2}}{\left(1 + \left(\frac{\partial f}{\partial \rho}\right)^2\right)^{3/2}}, \tag{53}$$

and

$$c_S = \frac{\frac{1}{\rho}\frac{\partial f}{\partial \rho}}{\left(1 + \left(\frac{\partial f}{\partial \rho}\right)^2\right)^{1/2}}. \tag{54}$$

These expressions are exact for aspheric surfaces with rotational symmetry, as represented by Eq. (50).

Let us now study with more detail these curvatures for surfaces with nearly rotational symmetry. For these surfaces, both curvatures, tangential and sagittal, are constant for all values of θ and a given value of ρ. In other words, the sagittal and the rotational maps are rotationally invariant. Now, by observing Fig. 13, we see that the axial (or sagittal) curvature $c_s = 1/r_s$ is the curvature at a point on the intersection of the optical surface with a plane passing through the local center of curvature, which is perpendicular to the plane containing the optical axis (a tangential plane). Thus, when the optical surface has rotational symmetry, the sagittal (or axial)

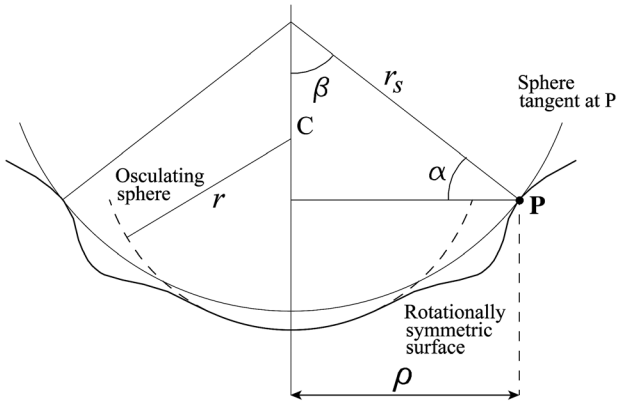

Fig. 13 An optical surface with rotational symmetry, showing the osculating sphere and also a sphere touching the aspherical surface along a ring passing through the point **P**.

radius of curvature can be calculated by tracing a ray passing through the point **P** and measuring its distance to the intersection with the optical axis. This is the reason for the name "axial curvature." If the optical surface does not have rotational symmetry, the ray passing through point P does not cross the optical axis. This effect is called skew ray error in the optometric literature.[29]

When the surface has rotational symmetry about the optical axis, these tangential and sagittal curvatures can be calculated with simpler formulas. In Fig. 13, we have a sphere tangent to a surface with rotational symmetry about the optical axis. The point of tangency is at the point **P** and along a circle containing the point **P**, concentric with the optical surface. Since the sphere and the surface are tangent along this circle, a line being perpendicular to the optical surface is also a radius for the sphere with the axial curvature $1/r_s$

$$c_S = \frac{1}{r_s} = \frac{\sin\beta}{\rho} = \frac{\tan\beta}{\rho[1+(\tan\beta)^2]^{1/2}}, \tag{55}$$

and using the theorem of Meusnier in Eq. (6)

$$c_S = \frac{1}{r_s} = \frac{\cos\alpha}{\rho} = \frac{1}{\rho[1+(\tan\alpha)^2]^{1/2}}. \tag{56}$$

These expressions are exact only for rotationally (axially) symmetric optical surfaces, without any nonrotationally symmetric aberrations.[29]

Barbero[30] has described the concepts of geodesic curvature and geodesic torsion as a metric of the difference between a rotationally symmetric and a nonrotationally symmetric surface. When nonrotational symmetric aberrations are present and this expression is used, important errors appear, mainly at the periphery of the corneal surface.

In the case of surfaces with symmetry of revolution, these are the tangential and the sagittal curvatures. For surfaces without symmetry of revolution, like the sphero-cylindrical surfaces or astigmatic corneas, in general, the principal curvatures are not in the tangential and sagittal directions. Thus, these principal curvatures are not the same as the averages of the tangential and sagittal curvatures, unless the surface or wavefront deformations are rotationally symmetric.

In surfaces without rotational symmetry, the two curvatures, sagittal and tangential, are completely independent of each other. Under these conditions, it is not possible to derive one type of curvature from the other. There is a lot of confusion in the literature about this topic. However, for surfaces with rotational symmetry, these two curvatures are related to each other as described by Klein and Mandell,[31] Tang et al.,[32] and Schwiegerling,[5] page 45)

$$c_t = \frac{d(\rho c_s(\rho))}{d\rho} \quad \text{or} \quad c_s(\rho) = \frac{1}{\rho}\int_0^S c_t(\rho')\mathrm{d}\rho'. \tag{57}$$

These expressions are also valid for aberrated surfaces as long as the aberrations are rotationally symmetric, or the nonrotationally symmetric aberrations are extremely small compared with the rotationally symmetric component. The local astigmatism axis has its axis is along with the tangential or sagittal directions only if the surface is rotationally symmetric.

When the surfaces do not have rotational symmetry, the two principal curvatures are not the same as the tangential and sagittal curvatures, at any point in the optical surface, which is the case when: (a) the surface has a cylindrical or sphero-cylindrical shape, (b) when the aberration surface has nonrotationally symmetric deformations.

In general, the principal curvatures cannot be calculated from the sagittal and tangential curvatures only. An extra parameter must be determined at all points in the optical surface, e.g., the orientation of the principal curvatures (cylinder axis) of the difference of their magnitudes (cylinder magnitude), or a curvature in another direction. This means that the sagittal and tangential maps do not provide the whole information about the shape of the surface deformations nor about the curvatures.

Examples of maps for tangential and sagittal curvatures, obtained by computer generation for an astigmatic (sphero-cylindrical) wavefront are in Fig. 14.

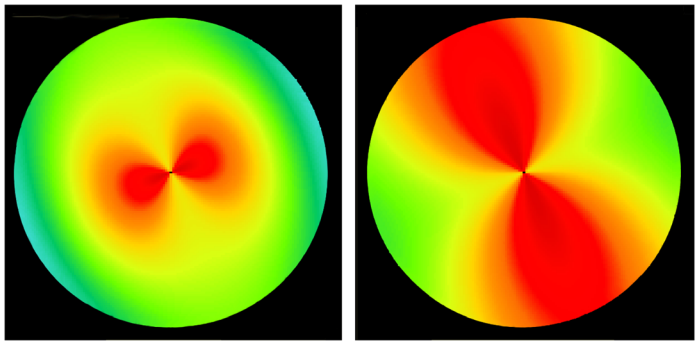

Fig. 14 An example of tangential map of curvatures (a) and a sagittal map of curvatures (b) for a sphero-cylindrical optical surface or wavefront. The color indicates the sign, red for positive values and green for negative values.

10.1 *Sagittal and Tangential Curvatures for Conic Surfaces*

Conic surfaces are a particular case of surfaces with rotational symmetry. For conic surfaces, the sagittal, azimuthal, or axial curvature is given by[33]

$$c_s = \frac{c}{[1 - Kc^2S^2]^{1/2}}, \tag{58}$$

and the tangential, radial, or instantaneous curvature is given as

$$c_t = \frac{c}{[1 - Kc^2S^2]^{3/2}}. \tag{59}$$

As in any rotationally symmetric surface, the two curvatures, sagittal and tangential, are related to each other. In this case, they are related as

$$c_s^3 = c^2 c_t, \tag{60}$$

where c is the vertex curvature, i.e., the curvature at the intersection of the optical surface with its optical axis. The local radius of curvature is equal to the radius of curvature r plus the aberration of the normal, represented by Δr, as illustrated in Fig. 15. Since the slope of the line going from the point **P** to the local center of curvature is equal to the first derivative or slope of the aspherical surface, the aberration of the normal can be obtained as

$$\Delta r = \frac{S}{\left(\frac{dz}{dS}\right)} + z - r, \tag{61}$$

which, for conic surfaces becomes

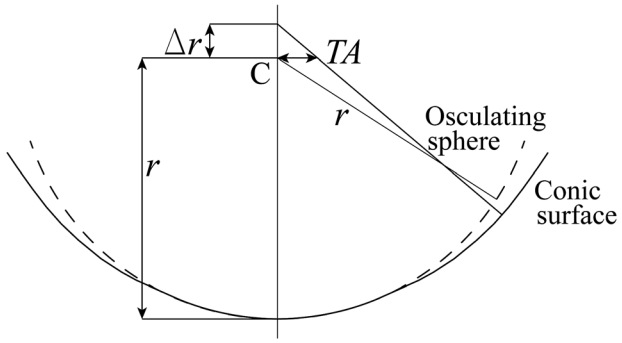

Fig. 15 A conic surface with its osculating sphere, illustrating the transverse aberration.

$$\Delta r = -Kz. \tag{62}$$

The anterior surface of the cornea is frequently assumed to be ellipsoidal, with or without rotational symmetry.[34,35] With this fact in mind, Harris,[36] and later Bektas,[37] studied the curvature of general ellipsoids using the fundamental form of surfaces. A detailed study of the shape of the cornea and its local curvatures has also been reported by Griffits et al.[38,39]

10.2 *Curvatures in Convex or Concave Optical Surfaces*

A particular case of special interest is the measurement of local curvatures in a strong spherical convex or concave with relatively small aberrations. It is also important to consider what happens when an unaberrated convergent or divergent wavefront is reflected or refracted in an aberrated optical sphere to measure this optical surface. In the case or reflection, the reflected wavefront will have the same aberrations as the incident wavefront, multiplied by two, and in the case of refraction, the refracted wavefront also will have the same aberrations but multiplied by $(n-1)$ which is close to 0.5. A consequence is that the local curvatures at all points over the wavefront the local curvatures after reflection or refraction are scaled by the same factor 2 or $(n-1)$.

It is important to notice that if a spherical or conic optical surface is aberrated, those aberrations could be defined and measured in a direction parallel to the optical axis or perpendicularly to a close reference sphere. Thus, we define the absolute aberrations as those in a direction parallel to the optical axis and the relative aberrations as those measured perpendicularly to the close reference sphere. Figure 16 illustrates these concepts of the absolute distance z_a and the relative distance z_r. They are related as

$$z_r = z_a \cos\theta, \tag{63}$$

where θ is the angle between their normal to the sphere and the normal to the aberrated sphere. If the aberrated wavefront is almost flat, the reference sphere is a plane and θ is zero.

The importance of this distinction can be clearly seen when we change the curvature of the reference sphere of a convex (divergent) wavefront by means of a collimating lens. By use of the Fermat principle, we can see that if the relative sagitta in the incident nearly spherical wavefront becomes equal to the absolute sagitta in the collimated wavefront. In Fig. 17, z_{r1} is the relative aberration in the divergent wavefront and it is equal to the absolute aberration z_{a2} in the collimated wavefront.

An interesting conclusion is that if we measure or evaluate the local curvatures in the convex or concave optical surface in Fig. 16 or the convergent wavefront in Fig. 17, the slope is large and thus we must use the exact Eq. (21) to calculate the local curvatures. On the other hand, if we need to calculate the relative local curvatures of the curvatures in the collimated wavefront in Fig. 17, we can use the simplified formula, in Eq. (20), or if the aberrations are not extremely large, even just the numerator in this expression, which can be written as

$$c_\alpha = \frac{1}{2}\left(\frac{\partial^2 f}{\partial x^2} + \frac{\partial^2 f}{\partial y^2}\right) + \left[\frac{1}{4}\left(\frac{\partial^2 f}{\partial x^2} - \frac{\partial^2 f}{\partial y^2}\right)^2 + \left(\frac{\partial^2 f}{\partial x \partial y}\right)^2\right]^{1/2} \cos 2(\alpha - \psi), \tag{64}$$

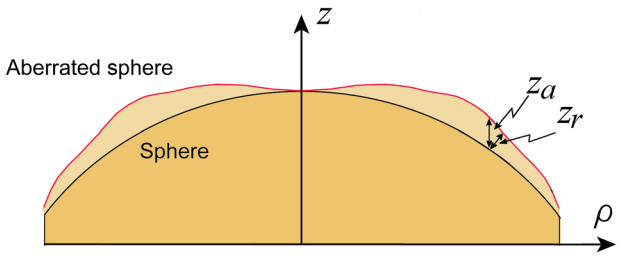

Fig. 16 Illustration of the absolute distance, measured with respect to the reference sphere, in a direction parallel to the optical axis and the relative distance, measured with respect to the reference sphere and in a direction towards the center of the sphere.

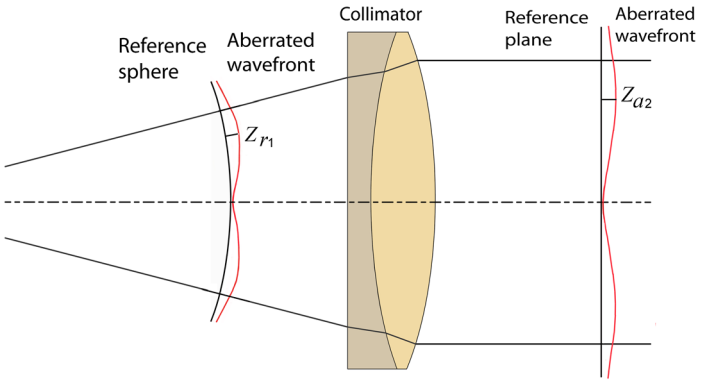

Fig. 17 Flattening of the curved, aberrated wavefront by means of a collimator.

which is valid for any almost flat (collimated) wavefront. Then, the local curvature along the x and y axes are given as

$$c_x = \frac{\partial^2 f}{\partial x^2} \quad \text{and} \quad c_y = \frac{\partial^2 f}{\partial y^2}. \tag{65}$$

The principal curvatures κ_1 and κ_2 can be obtained from Eqs. (21) and (23), as follows:

$$\kappa_1, \kappa_2 = \left(\frac{\partial^2 f}{\partial x^2} + \frac{\partial^2 f}{\partial y^2}\right) \pm \left[\left(\frac{\partial^2 f}{\partial x^2} - \frac{\partial^2 f}{\partial y^2}\right)^2 + 4\left(\frac{\partial^2 f}{\partial x \partial y}\right)^2\right]^{1/2}, \tag{66}$$

with an axis orientation given by Eq. (24).

11 Wavefront Sensing

All preceding treatment of local curvatures assumes that the analytic representation of the surface is known, otherwise, the surface must be measured and mathematically represented to calculate its local curvatures. Optical surfaces can be directly measured optically or mechanically in many ways, typically by profilometry, as described by Schmit et al.[40] In a more common method, optical surfaces and general optical components are evaluated by measuring the wavefront deformations in the reflected and/or refracted light beam in these systems. This procedure is normally called wavefront sensing, traditionally employed to test all types of optical systems[28] and also used to examine the eye,[41,42] mainly since the advent of adaptive optics. In many of these methods, it should be taken into account that nearly always a perfectly nonaberrated wavefront when reflected or refracted in even a perfect optical surface or system becomes aberrated, as described in optical design books.[43]

11.1 *Wavefront Sensing Devices*

Wavefront sensing devices retrieve the shape of wavefront $W(x, y)$ by measuring

1. Direct sensing of the wavefront phase, also known as the wavefront sagitta.
2. By measuring the wavefront slopes, or the transverse aberrations, which are related as

$$\frac{\partial W(x, y)}{\partial x} = -\frac{TA_x}{r_w}, \quad \frac{\partial W(x, y)}{\partial y} = -\frac{TA_y}{r_w}, \tag{67}$$

   where r_w is the distance from the observation plane to the screen with the cells or the array of virtual images and TA_x and TA_y are the distances from the actual ray and the reference ray when they cross the observation plane.[28]
3. By measuring the local curvatures at the wavefront surface.

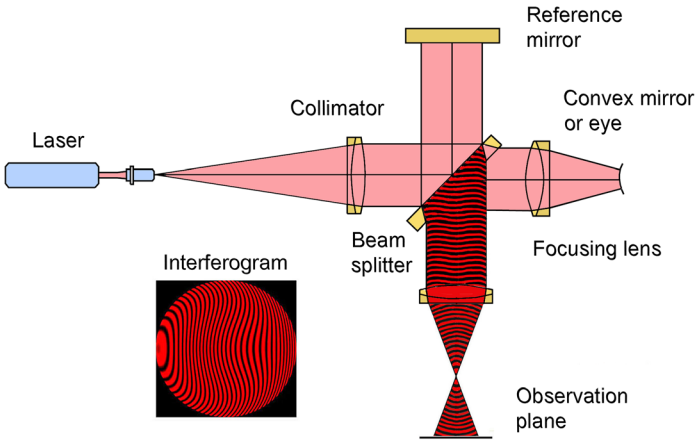

Fig. 18 Twyman–Green interferometer.

11.2 *Interferometric Wavefront Sensing*

The devices that can measure directly the wavefront deformations are the interferometers, which produce interferograms, representing curves of equal level, that can be processed to retrieve the slope and the local curvatures.[44] Two typical examples are the Fizeau[45] the Twyman–Green[46,47] interferometers (see Fig. 18).

Interferometers have an extremely large sensitivity to small deformations. As a result, the atmospheric turbulence, vibrations, and small movements make the system quite unstable. Interferometers that cancel out these vibrations and rapid movements had been designed,[48] making them more appropriate for ophthalmologic and optometric studies. This Twyman–Green interferometer uses the phase-shifting technique with four-phase steps taken simultaneously. To achieve this simultaneity, every pixel of the CCD image detector where the interferograms are imaged is formed by four pixels. Each cell has a polarizing layer on top, with different orientations for the linear polarization in each of them, as shown in Fig. 19. Since the light beam arriving in this image detector is circularly polarized, we have four different phase shifts. In all interferometer setups, the cornea or the retina under examination should be conjugate to the observation plane with the light detector.

11.3 *Foucault or Schlieren Wavefront Sensing*

In the Foucault test,[49] also known as Schlieren, when used to detect the flow of fluids or air turbulence, illustrated in Fig. 20, a knife edge is inserted perpendicularly to the point of

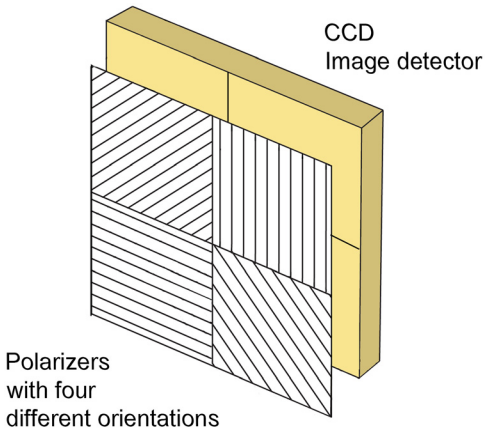

Fig. 19 Image detector for a vibration and turbulence stabilized Twyman–Green. The light beam arriving at this image detector is circularly polarized to have four different phase shifts.

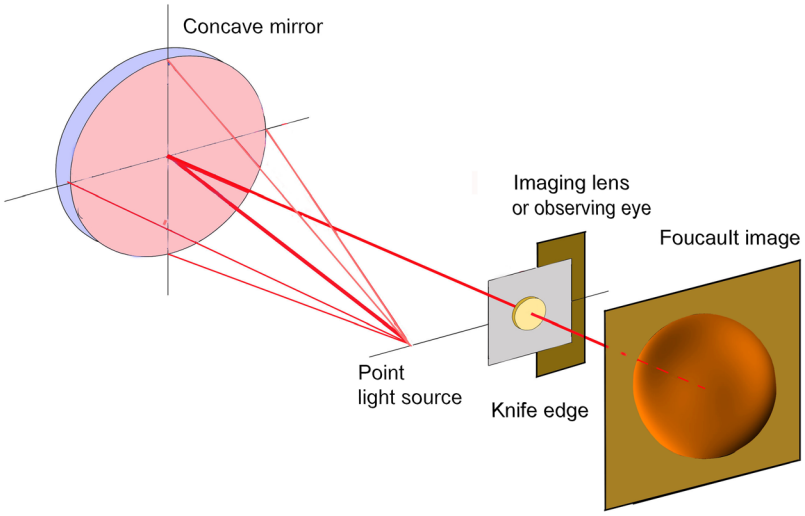

Fig. 20 Foucault test of a concave mirror.

convergence of the light coming back from a concave mirror, to block the ray lights that have a transverse aberration larger than the distance from center of the image to the edge of the knife edge. An imaging lens or an observing eye is located after the knife, to form an image of the mirror at an observing plane. The image in the observing plane has darker zones where the light rays are blocked. An image that subjectively illustrates the surface with the irregularities is clearly shown. This test measures the transverse aberrations, which are the same, except for a constant, to the surface slopes in a direction perpendicular to the knife edge. This test can be made quantitative.

The imaging lens in contact with the knife, should form at the observation plane an image of exit pupil of the system or the optical surface under test.

11.4 *Pyramidal Prism Wavefront Sensing*

An important modification of the Foucault test is obtained by substituting the knife edge with a pyramidal prism to simultaneously produce four Foucault images, with the edges of the four prisms forming the pyramid, as if four knives were introduced instead of just one.[50–55] This makes the test bidimensional, measuring the transverse aberration in the x- and y-direction. Also, the pyramidal prism has oscillations in both directions to measure the transverse aberrations over the whole aperture.

After obtaining the maps for the transverse aberrations TA_x and TA_y, the wavefront deviations are obtained. With this information, the local curvatures can also be retrieved. Let us assume that the illumination (irradiance) values on the images A, B, C, and D are $I_A(x,y)$, $I_B(x,y)$, $I_C(x,y)$, $I_D(x,y)$. The total amount of light on each of these images is directly proportional to the light passing through the corresponding quadrant in the pyramidal prism. Then, it is easy to show that the irradiance of these images can be added in pairs, obtaining four Foucault images, as if they were produced by four different knife orientations. If we add all four Foucault images, a uniformly illuminated image is obtained (see Fig. 21).

For any position of the pyramidal prism oscillation, we can measure two signals, $S_x(x,y)$ and $S_y(x,y)$, defined as

$$S_x(x,y) = \frac{(I_B(x,y) + I_D(x,y)) - (I_A(x,y) + I_C(x,y))}{I_A(x,y) + I_B(x,y) + I_C(x,y) + I_D(x,y)},$$
$$S_y(x,y) = \frac{(I_C(x,y) + I_D(x,y)) - (I_A(x,y) + I_B(x,y))}{I_A(x,y) + I_B(x,y) + I_C(x,y) + I_D(x,y)}, \tag{67}$$

where each of these irradiance values for every image pixel, are between zero and one. Then, the values of these signals are directly proportional to the difference between the two complementary

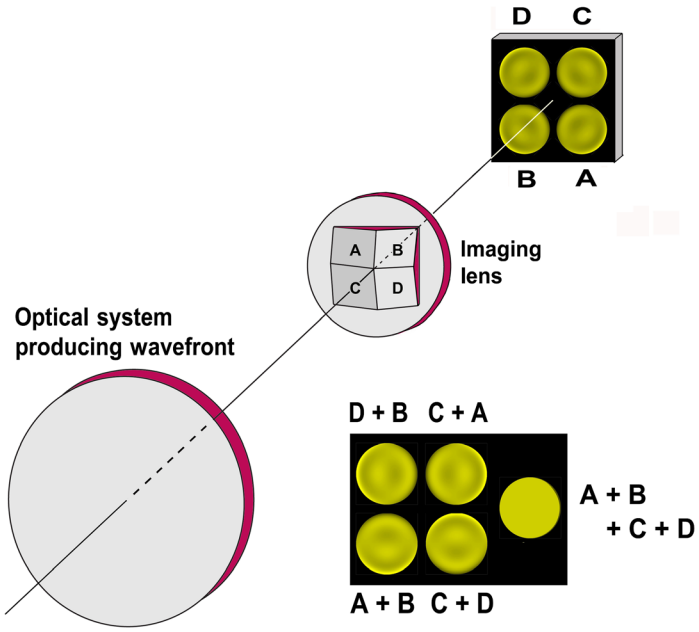

Fig. 21 Pyramidal prism wavefront sensor.

irradiance values for two knife orientations in opposite directions, producing values between -1 and $+1$, being zero when the two complementary irradiances are equal.

These signals are directly proportional to the slopes in the wavefront. If we represent by δV_x and δV_y the amplitudes of the oscillations of the pyramidal prism in the x- and y-directions, respectively, the wavefront slopes, from Eq. (67), can be shown to be

$$\frac{\partial W(x,y)}{\partial x} = \frac{r_w}{\delta V x} S_x(x,y), \quad \frac{\partial W(x,y)}{\partial y} = \frac{r_w}{\delta V y} S_y(x,y), \tag{69}$$

where r_w is the distance from the wavefront pupil to the pyramidal prism. The next step is to use Eq. (62) to find the transverse aberration values.

The imaging lens in contact with the pyramidal prism should form at the observation plane an image of exit pupil of the system, the pupil of the observed eye or the optical surface under test.

11.5 *Ronchi Wavefront Sensor*

Another wavefront sensor that measures the transverse aberrations (slopes) in one direction is the Ronchi test,[56] as in Fig. 22. It can be considered as a Foucault test, where the knife edge is substituted by a linear array of edges, implemented by a relatively coarse ruling with about 80 to 100 lines per inch.

This test was originally designed to evaluate concave mirrors, but it can be used to measure any kind of image forming optical devices, including the human eye. The exit pupil of the optical system must be conjugate to the observation plane.

11.6 *Interferometric Lateral Shearing Wavefront Sensing*

Other sensors that measure the slopes in one direction are the lateral shear interferometers, with many possible configurations, where the two interfering wavefronts are laterally displaced one respect to the other,[57] as in Fig. 23. The interferograms measure the wavefront slopes in the direction of the shear. Both wavefronts have exactly the same deformations.

Figure 23 illustrates a lateral shear interferometer with high fringe stability that requires a He–Ne laser as the illuminating light source. The exit pupil of the optical system of the human

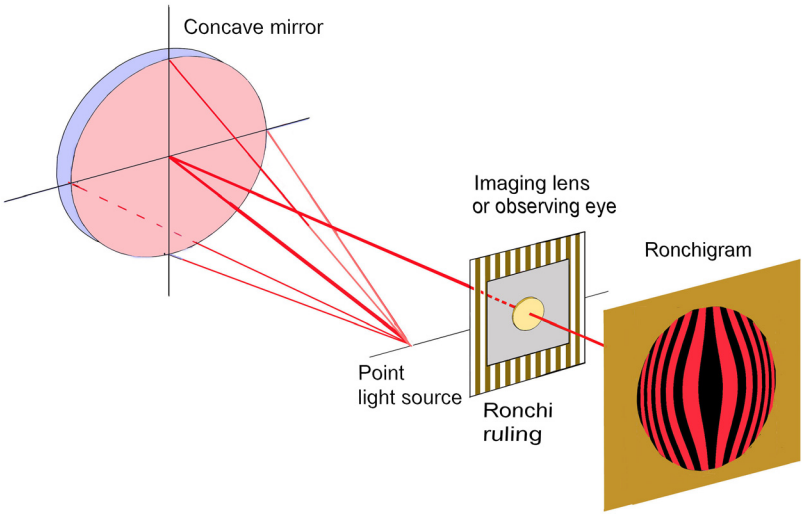

Fig. 22 Ronchi test.

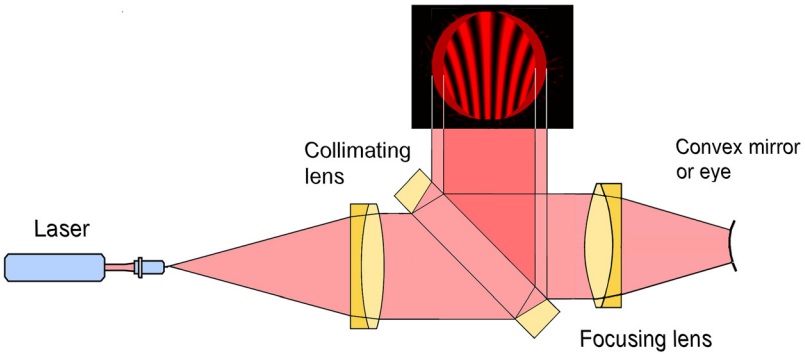

Fig. 23 Lateral shear interferometer.

eye under examination must be in a plane conjugate to the observation plane. The necessary optical components to achieve that condition must be used.

Another example of this type of interferometer can be constructed with a Mach–Zehnder interferometer[58] with one of its mirrors slightly rotated to laterally displace one of its two interfering images. In these interferometers, the interference fringes represent the wavefront slopes in the direction of the lateral shear. It is interesting to know that a Ronchi test could be considered as a relatively low sensitivity lateral shearing interferometer where the lateral shear depends on the frequency of the ruling.

11.7 *Inverse Ronchi and Deflectometry Wavefront Sensing*

The Ronchi test was invented to test convergent wavefronts. However, it can be adapted to test convex surfaces, e.g., the cornea of the human eye. It could be named the inverse Ronchi test, with a configuration as in Fig. 24. There are several differences with the classic Ronchi test: (1) convex instead of concave surfaces are evaluated, (2) all the system is on-axis, and (3) a linear array of light sources is used instead of a point light source. This system is seldom used; an inverse Hartmann test is generally preferred to have a two-dimensional analysis and measure the wavefront slopes in two dimensions. Ideally, the array of light strips should be concave, as in the inverse Hartmann configuration in Fig. 27.

The sensitivity and accuracy of this test can be increased by measuring the Ronchi fringes with respect to a reference ideal Ronchi pattern with straight, equidistant, and parallel fringes with approximately the same period, forming a pattern of moiré fringes. This arrangement is frequently known as deflectometry. The reference ruling can be a pattern of circular fringes,

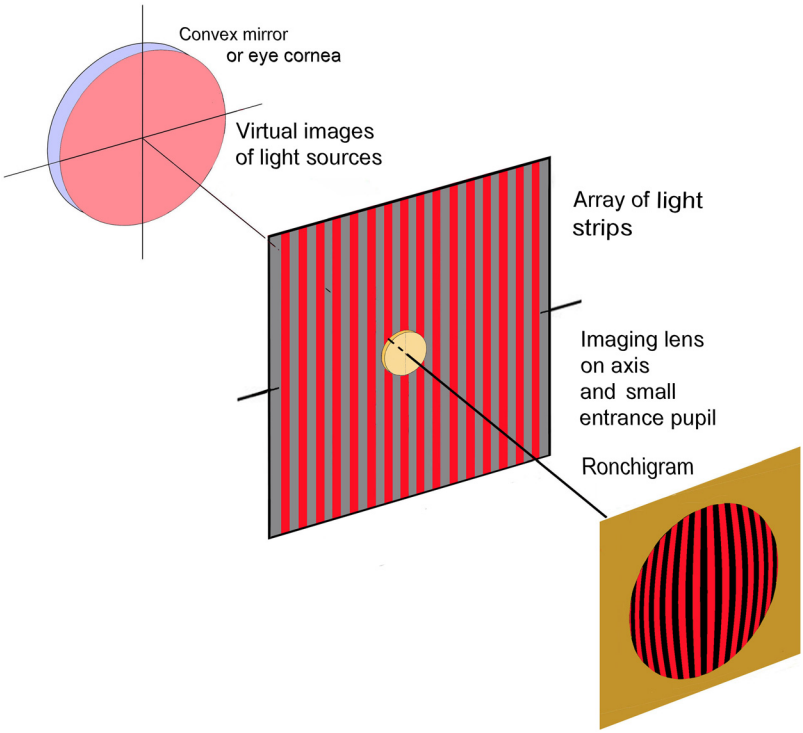

Fig. 24 Inverse Ronchi test.

like in a defocused fringe pattern. A study with this method to measure the curvature of a small convex spherical mirror has been reported by Hong et al.[59]

All of these methods that measure transverse aberrations have a strong similarity with lateral shearing interferometry and all devices that produce fringes representing the slope of the wavefront (or transverse aberration) in the direction perpendicular to the fringes. All slope-measuring devices, like these ones, require a minimum of two measurements in two different directions to obtain the slopes in all directions. It is simple to show from Eq. (67) that if two contiguous Ronchi fringes are separated by Δx and ΔTA_x the separation between two lines on the ruling, then we can write the curvature along the perpendicular to the fringes as

$$c_x = \frac{\partial^2 W(x,y)}{\partial x^2} = -\frac{1}{r_w}\frac{\Delta TAx}{\Delta x}, \tag{70}$$

where r_w is the distance from the exit pupil to the Ronchi ruling. In other words, the curvature along the perpendicular to the fringes is inversely proportional to the period (separation of the fringes.

11.8 *Tscherning and Hartmann Wavefront Sensing*

Tscherning[60] in 1894 published his results on the measurement of the human eye aberrations. He placed a small light source in front of the patient at several meters distance, with a 2.00 diopters lens in front of his eye to defocus its image. Close to the lens a grid of lines or holes was located. The pattern of lines or dots observed by the patient was an indication of the aberrations of the eye. In recent years Mrochen et al.[61] designed an aberrometer based on Tscherning principles using modern tools.

Another aberrometer based on a similar method, using laser ray tracing was devised by Navarro and Losada[62] where a thin laser beam is projected onto the retina in a sequential manner and the direction of the ray coming out from the eye is measured.

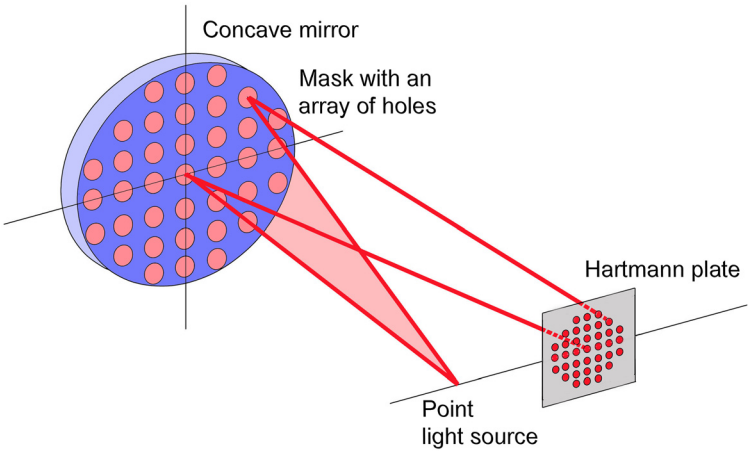

Fig. 25 Hartmann test.

A few years later than Tscherning, Hartmann in 1900 published his proposal for another test based on a similar method.[63] Several different optical arrangements based on the Hartmann test have appeared[64,65] as illustrated in Fig. 25.[66]

11.9 *Inverse Hartmann Wavefront Sensing*

If the surface under test is convex instead of concave, the light from a point source cannot converge to implement the Hartmann test. Instead, the optical arrangement in Fig. 26 can be used, which can be considered as an inverse Hartmann test where the Hartmann plate with many bright spots is replaced by an array of light sources and the point light source by a small aperture optical system. This system works on-axis, instead of slightly off-axis as in the Hartmann test.

The optical system illustrated in Fig. 27 is used mostly to measure the convex cornea of the human eye. In this system, the virtual images of the light sources are formed on a slightly curved surface behind the corneal surface. If the ovoidal surface containing the light sources is

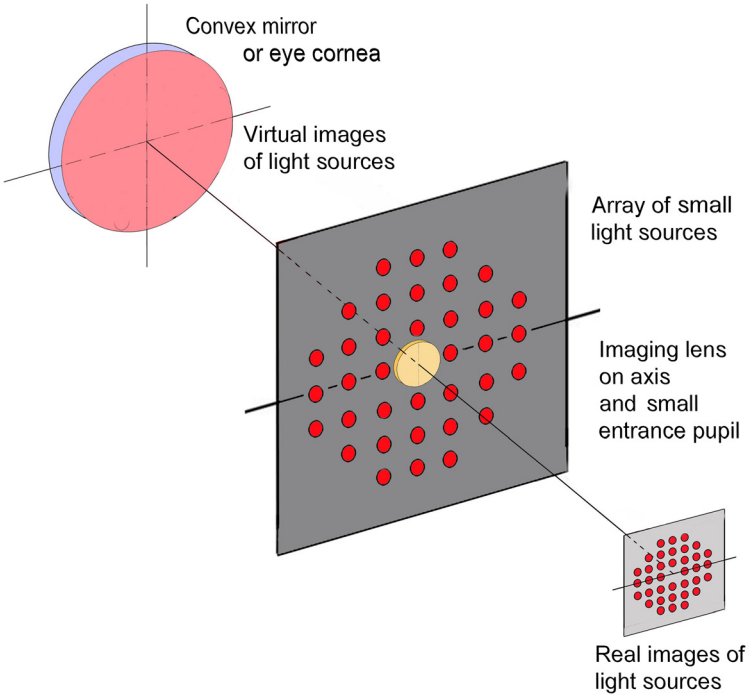

Fig. 26 Inverse Hartmann test.

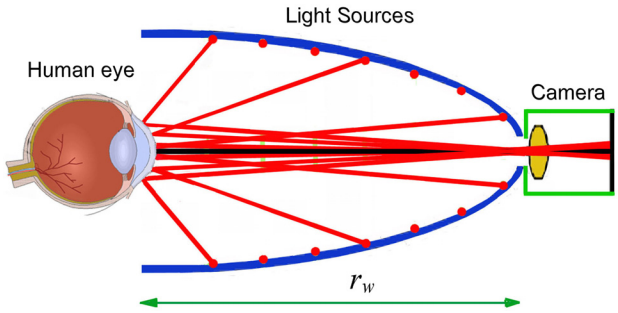

Fig. 27 Inverse Hartmann configuration with the array of light sources in a curved concave surface, used to measure the cornea of the eye of the human eye.

appropriately elongated, the images are in a plane.[66] Frequently, a compromise is taken so that the ovoidal surface is not too elongated and the virtual image surface is not too curved, by making the support for the light sources or Placido rings concave, almost paraboloidal. The camera forms at its focal plane a real image of the light sources to measure the transverse aberrations.

The light sources can be distributed in arrays with different configurations, as in Fig. 31, but the most common for this kind of instruments is with Placido rings. The only problem with the rings is the presence of the skew ray error due to the low sensitivity of them to transverse errors in a direction perpendicular to the diameters in the circular pupil. However, several different approaches had been used to eliminate this error,[29] e.g., Gómez-Tejada et al.,[67] dividing the pupil in hexagonal cells and using an iterative process.

11.10 *Shack–Hartmann Wavefront Sensing*

If the wavefront to be measured is small and nearly flat, the implementation of the Hartmann test is not simple. Then, another important modification to the Hartmann test was invented by Platt and Shack[68] and known as the Shack–Hartmann test, as in Fig. 28. Convergent wavefronts can also be measured if a small collimator is used in the convergent beam.

The range of curvature values that can be measured with them had been studied by Campbell.[69] The Shack–Hartmann sensor can be adapted to measure in a differential manner, by measuring three times each square cell, as illustrated in Fig. 29. With these three measurements, with three different positions for the Shack–Hartmann plate, the local principal curvatures can be easily and accurately evaluated.[70]

The Shack–Hartmann is used to measure the wavefront aberrations in the human eye, as in Fig. 30. Local wavefront curvatures can be measured with Shack–Hartmann wavefront sensors. The planes at $\mathbf{P}_1$ and $\mathbf{P}_2$ are conjugates.

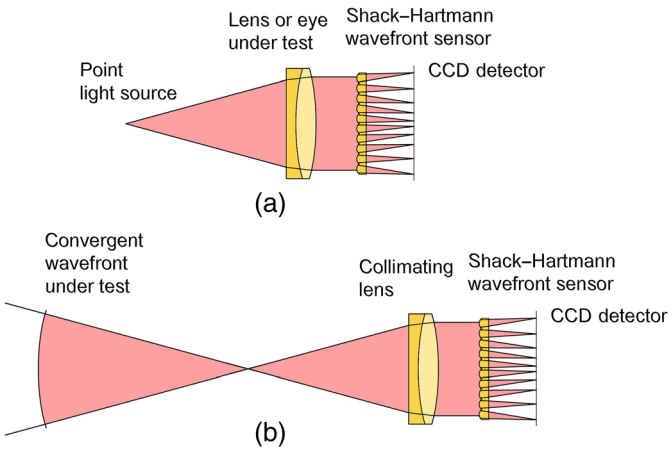

Fig. 28 Shack–Hartmann test.

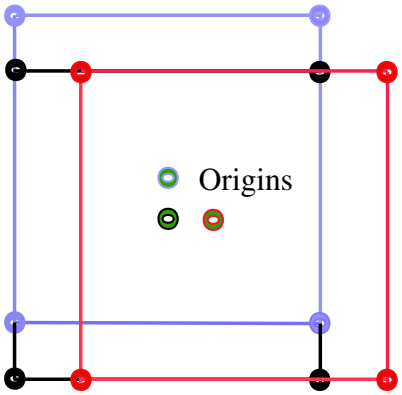

Fig. 29 Measuring a Shack–Hartmann square cell in two orthogonal directions and one without displacement, to measure the principal curvatures.

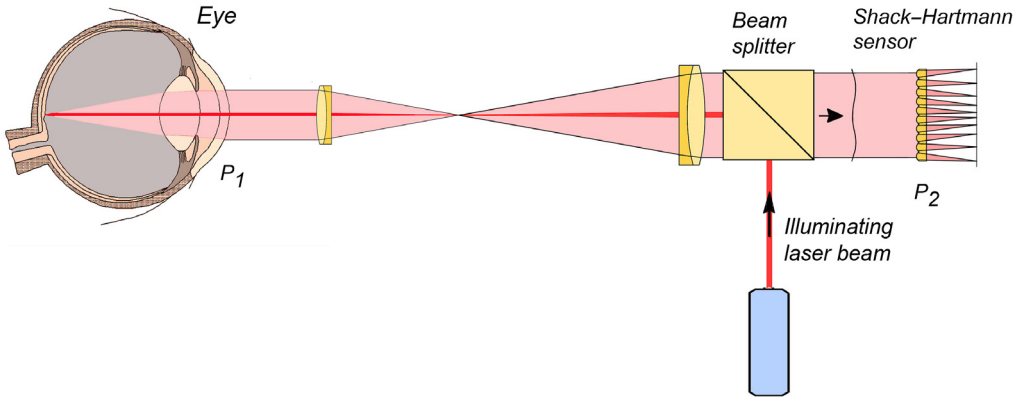

Fig. 30 Optical configuration to measure the eye aberrations with the Shack–Hartmann test.

11.11 *Sampling Screens in Hartmann and Inverse Shack–Hartmann Devices*

In the inverse Hartmann type configurations, the array of light sources can have several possible array configurations, as illustrated in Fig. 31.

In astronomical optical surfaces testing the most common array is with square cells, as in Fig. 31(a). In ophthalmic instruments, such as corneal topographers, the most common array of light source is with Placido rings in Fig. 31(d). However, all these light arrays can be used with any system. The simplest one for curvature measurements is the array of squares, with integration methods as described by Ghozeil and Simmons[71] and by Southwell.[72] Hexagonal patterns had been integrated by Gantes-Nuñez et al.[73] and Placido rings by Gómez-Tejada et al.[67]

11.12 *Processing Hartmann and Shack–Hartmann Wavefront Sensors Data*

In most optical Hartmann type arrangements, the reference surface used to find the reference points for the measurement of the transverse aberrations is a perfectly spherical surface, close to the aberrated real surface. Thus, the measured transverse aberrations are produced by the separation between the aberrated surface and the spherical reference surface, measured perpendicularly to this reference surface.

The transverse aberrations are directly proportional to the slopes of the optical surface or wavefront in a square cell, as shown in Fig. 32. These aberrations are the angular separation between the actual reflected or refracted ray and the path for the ideal ray. This ideal path for the reflected path is calculated for an ideal reference surface. If this reference surface is flat, the angle between the actual ray and the ideal ray is twice the slope of the surface at the point where the ray is reflected.

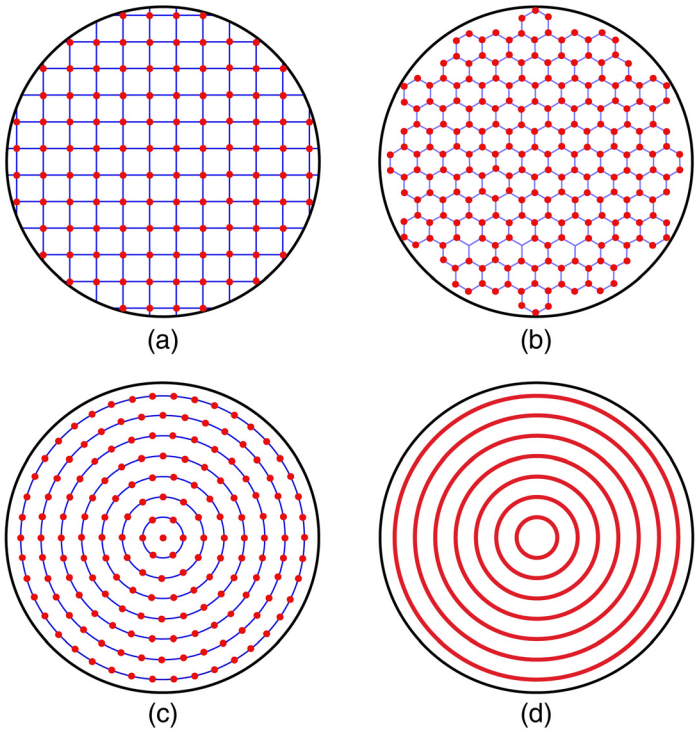

Fig. 31 Several possible arrays of light sources for Hartmann-type measuring systems. (a) Square cells, (b) hexagonal cells, (c) circular array of points sources, and (d) Placido rings.

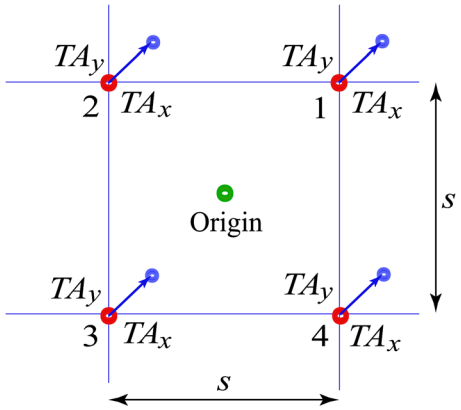

Fig. 32 Square cell with four points where the transverse aberrations are measured.

12 Calculation of Local Curvatures by Measurements of the Transverse Aberrations

From the exact expression in Eq. (21), we see that the local curvatures at any point in a surface can be calculated if the two first derivatives, respect to x and respect to y, the two second derivatives, respect to x and respect to y are known. So, the first step is to measure them.

The slopes or derivatives may be obtained by first obtaining the wavefront deformations in each cell in a procedure called zonal method. The reference optical surface deformations $z_r(x, y)$ over the square cell can be represented as

$$z_r(x, y) = A_1 x + A_2 y + A_3(x^2 + y^2) + A_4(x^2 - y^2) + 2A_5 xy, \tag{71}$$

and transforming to polar coordinates with $x = \rho \cos \alpha$ and $y = \rho \sin \alpha$

$$z_r(\rho,\alpha) = A_1\rho\cos\alpha + A_2\rho\sin\alpha + A_3\rho^2 + A_4\rho^2(\cos^2\alpha - \sin^2\alpha) + 2A_5\rho^2\cos\alpha\sin\alpha$$
$$= A_1\rho\cos\alpha + A_2\rho\sin\alpha + A_3\rho^2 + A_4\rho^2\cos 2\alpha + A_5\rho^2\sin 2\alpha. \tag{72}$$

If we define an angle ψ by $B\cos 2\psi = A_4$ and $B\sin 2\psi = A_5$ and, after some algebraic manipulation we obtain

$$z_r = A_1\rho\cos\alpha + A_2\rho\sin\alpha + A_3\rho^2 + B\rho^2\cos 2\psi\cos 2\alpha + B\rho^2\sin 2\psi\sin 2\alpha,$$
$$= A_1\rho\cos\alpha + A_2\rho\sin\alpha + A_3\rho^2 + (A_4^2 + A_5^2)^{1/2}\rho^2\cos 2(\alpha - \psi). \tag{73}$$

If the aberrations are small, the second derivative in the direction α will give the local curvature in that direction. The coefficients A_1 and A_2, have the same structure as Euler equation in Eq. (28). The astigmatic axis orientation is given as

$$\tan 2\psi = \frac{A_5}{A_4}. \tag{74}$$

The surface deformations are measured on top of the reference sphere, with origin at the center of the square cell. The first two terms are the relative tilts or slopes about the y and the x axes, the third term is a relative spherical deformation, approximated by this parabolic term, since the deformation is small, the fourth term is a cylindrical (astigmatic) relative deformation with axis along the x or y axis and the last term is a cylindrical (astigmatic) relative deformation with axis at ± 45 deg. Thus, the transverse aberrations are given as

$$-\frac{2}{r_w}TA_x = A_1 + 2A_3x + 2A_4x + A_5y,$$
$$-\frac{2}{r_w}TA_y = A_2 + 2A_3y - 2A_4y + A_5x. \tag{75}$$

It is possible to prove that if the eight transverse aberrations, two at each corner of the square cell are measured, in principle eight coefficients can be determined. However, the eight measurements are not all independent, but there is enough information to find an accurate solution for tilts, defocus, and astigmatism, including its axis orientation,[73] obtaining

$$A_1 = -\frac{1}{4r_w}(TA_{x1} + TA_{x2} + TA_{x3} + TA_{x4}),$$
$$A_2 = -\frac{1}{4r_w}(TA_{y1} + TA_{y2} + TA_{y3} + TA_{y4}),$$
$$A_3 = -\frac{1}{8sr_w}(TA_{x1} + TA_{y1} - TA_{x2} + TA_{y2} - TA_{x3} - TA_{y3} + TA_{x4} - TA_{y4}),$$
$$A_4 = -\frac{1}{8sr_w}(TA_{x1} - TA_{y1} - TA_{x2} - TA_{y2} - TA_{x3} + TA_{y3} + TA_{x4} + TA_{y4}),$$
$$A_5 = -\frac{1}{8sr_w}(TA_{x1} + TA_{y1} + TA_{x2} - TA_{y2} - TA_{x3} - TA_{y3} - TA_{x4} + TA_{y4}), \tag{76}$$

where s is the length of one side of the square cell. Once the five coefficients are found, the first two, A_1 and A_2, are ignored.

If the aberration deformations are large, the transverse aberrations are also large and the difference between the reference surface slopes and the aberrated surface slopes may be so important that the denominator in Eqs. (20) or (21) may be quite different from one. Then, the following derivatives at the center of the square cell ($x = 0$; $y = 0$) are important:

$$\frac{\partial z_r}{\partial x} = A_1, \quad \frac{\partial z_r}{\partial y} = A_2, \quad \frac{\partial^2 z_r}{\partial x^2} = 2(A_3 + A_4), \quad \frac{\partial^2 z_r}{\partial y^2} = 2(A_3 - A_4), \quad \frac{\partial^2 z_r}{\partial x \partial y} = 2A_5. \tag{77}$$

Then, these derivatives are used in Eq. (21), obtaining the relative local curvatures as

$$c_\alpha = \frac{2(A_3 + (A_4^2 + A_5^2)^{1/2} \cos 2(\alpha - \psi))}{(1 + (A_1 \cos \alpha + A_2 \sin \alpha)^2)(1 + A_1^2 + A_2^2)^{1/2}}. \tag{78}$$

Another possible method that can be used in lenses is to directly measure the sagittal values at many points over the aperture with a mechanical or optical profilometer[40] and then to obtain an analytical expression for the optical surface shape. Then, the absolute local curvatures may be obtained with the exact expression in Eq. (21).

13 Direct Measurement of the Mean Curvature with the Irradiance Transport Equation

A method to directly measure the local curvatures was described by Roddier[74,75] and it is known as the method of the transport of irradiance. If a wavefront is collimated, almost flat, with relatively small aberrations, the local curvatures in the x and y directions are given just by the second derivatives as

$$c_x = \frac{\partial^2 W(x,y)}{\partial x^2} \quad \text{and} \quad c_y = \frac{\partial^2 W(x,y)}{\partial y^2}. \tag{79}$$

Half the Laplacian, defined as the semi-sum of these curvatures in Eq. (39) is the mean curvature. This expression is also known as the Poisson equation.

Now, let us consider a collimated and aberrated light beam propagating along an axis z, as in Fig. 33. In the regions where the light rays are denser, the irradiance is higher. As the light beam travels, the irradiance and the wavefront shape change continuously along the trajectory. Omitting the mathematical details (Malacara et al.[44]), it can be shown that if an aperture much larger than the wavelength is assumed, two equations are obtained, one for the change in the shape of the wavefront and another for the change in irradiance along the trajectory. For our purposes, the more important is the second, for the change in irradiance, given as

$$\frac{\partial^2 I(x,y)}{\partial z^2} = -\nabla I(x,y) \bullet \nabla W(x,y) - I\nabla^2 W(x,y). \tag{80}$$

This is the irradiance transport equation. According to Ichikawa et al.,[76] the terms contained in this equation represent the following. The gradient of the irradiance $I(x,y)$ represents the direction in which the irradiance change with more speed. The gradient of $W(x,y)$ is the direction and magnitude of the local wavefront tilt. The scalar product of these two gradients represents the irradiance variation along the optical axis due to the local wavefront tilt. For this reason, this is called a prism term. The last term in this equation is the irradiance along the z axis due to the local mean curvature. This is the lens term.

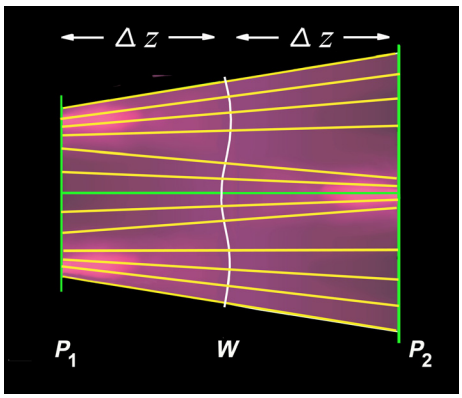

Fig. 33 Transport of irradiance. The irradiance distribution is different at two planes, equidistant from the aberrated wavefront.

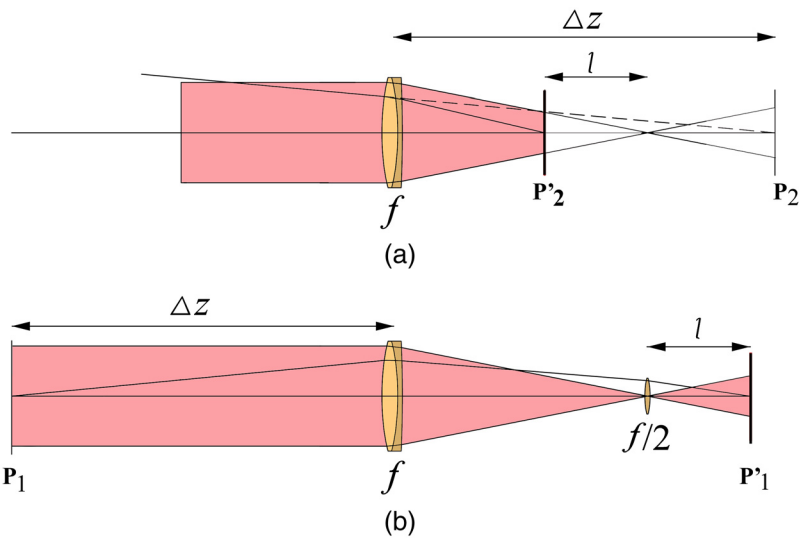

Fig. 34 (a) and (b) Location of the two planes $\mathbf{P}'_1$ and $\mathbf{P}'_2$, at equal distances $\pm l$ from the focus of the lens.

Roddier and Roddier[77] used these results to obtain the mean curvature at all points (x, y) in a wavefront, assuming that the illumination is constant over the pupil, obtaining the irradiance at two planes $\mathbf{P}_1$ and $\mathbf{P}_2$, symmetrically located respect to the pupil, as in Fig. 34 as

$$I_1(x, y, \Delta z) = I_0 + \left(\frac{\partial I(x, y, z)}{\partial z}\right)_{z=0} \Delta z, \tag{81}$$

and

$$I_2(x, y, \Delta z) = I_0 - \left(\frac{\partial I(x, y, z)}{\partial z}\right)_{z=0} \Delta z. \tag{82}$$

It can be seen that when the wavefront is perfectly plane at the pupil, the Laplacian at all point inside the pupil and the radial slope at the edge of the pupil are both zero, so that $I_1(x, y, \Delta z)$ is equal to $I_2(x, y, -\Delta z)$ but in general this is not the case. Then, the so-called sensor signal is

$$\frac{I_1(x, y, \Delta z) - I_2(x, y, -\Delta z)}{I_1(x, y, \Delta z) + I_2(x, y, -\Delta z)} = \frac{1}{I_0}\left(\frac{\partial I(x, y, z)}{\partial z}\right)_{z=0} \Delta z. \tag{83}$$

On the other hand, after some considerations in the irradiance transport equation, as Roddier and Roddier[77] points out, we can obtain

$$\frac{I_1(x, y, \Delta z) - I_2(x, y, -\Delta z)}{I_1(x, y, \Delta z) + I_2(x, y, -\Delta z)} = \left(\frac{\partial W(x, y, z)}{\partial n}\delta_c - P(x, y)\nabla^2 W(x, y)\right)\Delta z, \tag{84}$$

where the first term inside the right hand parenthesis is the wavefront slope around the pupil edge $P(x, y)$ is the pupil's edge, and the last term is the Laplacian.

With this result, measuring the irradiance at these two planes symmetrically located with respect to the aberrated wavefront, the shape of the pupil can be found. Ideally, the two symmetric planes where the irradiance distributions must be measured are at distances $\pm\Delta z$ from the pupil at a lens with focal length f. In Fig. 34 these two planes are $\mathbf{P}_1$ and $\mathbf{P}_2$. The only practical problem is that the plane $\mathbf{P}_1$ is inaccessible. The solution is simple if an auxiliary lens with focal length $f/2$, is placed at the focus of the lens as illustrated in Fig. 34. Then, the conjugate of the plane $\mathbf{P}_1$ is at $\mathbf{P}'_1$. Conjugate planes have the same irradiance distribution, except for a scale factor equal to the lateral magnification at these planes. Then, the measurements are taken at two planes $\mathbf{P}'_1$ and $\mathbf{P}'_2$, which can be shown to be at equal distances $\pm l$ from the focus of the lens.

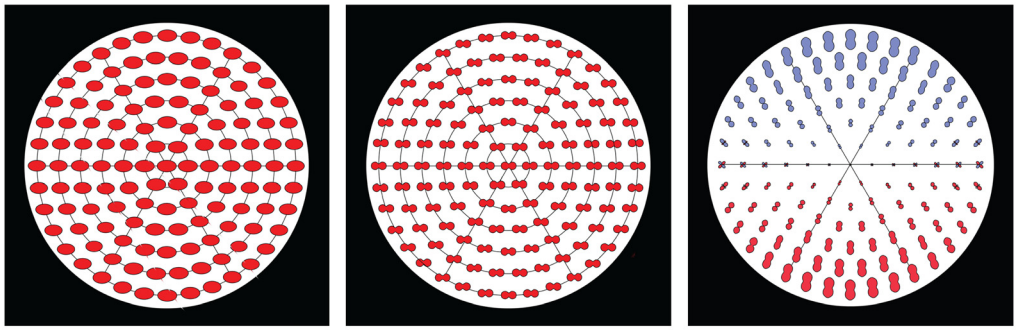

Fig. 35 Local curvature maps for an aberrated optical surface with some primary aberrations. (a) astigmatism and defocus, (b) astigmatism, and (c) coma (from Hernández–Delgado et al.[81]).

It can be easily shown that l and Δz are related by

$$\Delta z = \frac{f(f-1)}{l}. \tag{85}$$

Roddier and Roddier[77] points out that the small lens with focal length $f/2$ is not absolutely necessary. Thus, with two defocused images, one inside of focus and the other outside of focus, the wavefront mean curvatures can be obtained, i.e., the Laplacian. Roddier and Roddier[77] reported a method using successive iterations of Fourier transforms to calculate the wavefront shape from a knowledge of the Laplacian.

Another method to measure directly the curvature when the wavefront is nearly collimated and without strong slopes, was proposed by Paterson and Dainty,[78] using a quadrant detector. With the four measurements, one on each quadrant, any asymmetries in the small image of a point light source are used to calculate the mean curvature and two orthogonal slopes.

13.1 *Curvature Maps*

Curvature, vergence (degree of convergence or divergence) or power maps (in diopters), are an important representation on optometry and ophthalmology of optical surfaces, as described by Nam et al.,[79] Corbet et al.,[80] and Wang.[16]

Different manners to represent in a single map these parameters have been proposed, for example, some local curvature maps are illustrated in Fig. 35 using a representation where the three curvature parameters, i.e., spherical component, astigmatism and cylindrical axis orientation are shown in a single map, as described by Hernández-Delgado.[81] The sampling points must be uniformly distributed over the aperture, e.g., forming square or hexagonal cells. In these maps they are located in concentric circles, each one with a number of sampling points equal to six times the ring number. The red color represents positive local curvatures and blue color represents negative local curvatures.

14 Summary and Conclusions

Complete mathematical methods to calculate the local curvature as defined in the ophthalmology field have been described and we also proposed some practical calculations. We have shown that from a complete definition of local curvature (asymmetrical surfaces) a particular case (rotationally symmetric surfaces) can be derived making the angle of rotation constant. Corneal evaluation is usually made by calculating local curvatures. Calculations for particular cases such as the principal curvatures and the tangential, sagittal, principal, mean, and Gaussian local curvatures are derived in an intuitive and simple manner, obtaining highly accurate results, even for strongly curved surfaces and wavefronts. The results are valid for any kind of surface with or without rotational symmetry. The high importance of the concept of local curvatures in modern optics,

mainly in ophthalmology and optometry is described in detail, including some of the most common measurements used in ophthalmologic and optometric optics. In summarizing, we have made a complete review of the concepts and associated mathematics of local curvatures in an optical surface or wavefront and its applications to ophthalmic and optometric systems.

In the second part of this review, we describe the classical and modern main methods and devices for wavefront sensing, measuring elevations, slopes, or curvatures. We conclude with a description of some methods to measure and calculate local curvatures from wavefront sensors by measuring the wavefront elevations, the transverse aberrations (slopes), or directly the curvatures.

References

1. D. Margalit, *The History of Curvature*, Villanova University, https://www34.homepage.villanova.edu/robert.jantzen/maple/misc/history_of_curvature/k.htm (2008).
2. G. Bardini and G. M. Gianella, "A historical walk along the idea of curvature, from newton to gauss passing from Euler," *Int. Mathem. Forum* **1**, 259–278 (2016).
3. I. Newton, "Method of fluxions and infinite series, with its application to the geometry of curve-lines," Franklin Classics Trade Press (1736).
4. J. L. Coolidge, "The unsatisfactory story of curvature," *Am. Math. Month.* **59**, 375–379 (1952).
5. J. Schwiegerling, *Field Guide to Visual and Ophthalmic Optics*, SPIE Press, Bellingham, WA (2004).
6. M. W. A. Wijntjes, A. Sato, and V. Hayward, "Local surface orientation dominates haptic curvature discrimination," *IEEE Trans. Haptics* **2**, 94–102 (2009).
7. E. Luders et al., "A curvature-based approach to estimate local gyrification on the cortical surface," *NeuroImage* **29**, 1224–1230 (2006).
8. O. N. Stavroudis, *The Mathematics of Geometrical and Physical Optics*, Chapter 4, Wiley-VCH, Weinheim (2006).
9. J. J. Stoker, *Differential Geometry, Pure and Applied Mathematics*, Chapter 4, Vol. 20, p. 88, Wiley-Interscience, NY (1969).
10. M. M. Lipschutz, *Differential Geometry*, McGraw Hill, Book Co. (1971).
11. I. N. Bronshtein and K. A. Semendyayev, *A Guide Book to Mathematics*, Springer Verlag, New York (1973).
12. B. Kepr, "Differential geometry," in *Survey of Applicable Mathematics*, K. Rektorys, Ed., 2nd rev. ed., Kluwer Academic Publishers, Netherlands (1994).
13. A. Gray, E. Abbena, and S. Salamon, *Modern Differential Geometry of Curves and Surfaces with Mathematica*, 3rd ed., Chapman and Hall/CRC, New York, NY (2006).
14. T. Krauthammer and E. Ventsel, *Thin Plates and Shells. Theory, Analysis, and Applications with Mathematica*, Wolfram Research, Marcel Dekker, Boston, MA (2001).
15. S. Bergbauer and D. D. Pollard, "How to calculate curvatures of sampled geological surfaces," *J. Struct. Geol.* **25**, 277–289 (2003).
16. M. Wang and T. S. Swartz, *Corneal Topography*, 2nd ed., Slack, Inc., Thorofare, NJ (2012).
17. A. G. Kästner, *Anfangsgründe der Mathematik (Foundations of Mathematics)*, Nabu Press (1758).
18. J. Bernoulli, *Acta Eruditorum* (1691).
19. L. Euler, "Recherches sur la Courbure des Surfaces," *Memoires de l'academie des sciences de Berlin*, **16**, 119–143 (1767).
20. C. Truesdell, "Jean-Baptiste-Marie Charles Meusnier de la Place (1754-1793): an historical note," *Meccanica* **31**, 607–610 (1996).
21. J. Kneisly, "Local curvature of wavefronts in an optical system," *J. Opt. Soc. Am.* **54**, 229–235 (1964).
22. S. Bektas, "Generalized Euler formula for vurvature," *IJREAS* **6**, 292–304 (2016).
23. J. J. Koenderink and A. J. van Doom, "Surface shape and curvature scales," *Image Vis. Comput.* **10**, 557–564 (1992).

24. F. Nasrin, R. V. Iyer, and S. Mathews, "Simultaneous estimation of corneal topography, pachymetry, and curvature," *IEEE Trans. Med. Imaging* **37**, 2463–2473 (2018).
25. P. Roitman, "Gaussian curvature, mirrors and maps," *Am. Math. Monthly* **119**, 506–509 (2012).
26. E. M. Schiesser et al., "Gaussian curvature and stigmatic imaging relations for the design of an unobscured reflective relay," *Opt. Lett.* **43**, 4855–4858 (2018).
27. C. Roberts, "The accuracy of power maps to display curvature data in corneal photographic systems," *Invest. Ophthal. Vis. Sci.* **35**, 3525–3532 (1994).
28. D. Malacara, *Optical Shop Testing*, 3rd ed., Wiley Interscience, New York (2007).
29. S. A. Klein, "Axial curvature and the skew ray error in corneal topography," *Opt. Vis. Sci.* **74**, 931–944 (1997).
30. S. Barbero, "The concept of geodesic curvature applied to optical surfaces," *Opht. Physiol. Opt.* **35**, 388–393 (2015).
31. S. A. Klein and R. B. Mandell, "Axial and instantaneous power conversion in corneal topography," *Invest. Ophthalm. Vis. Sci.* **36**, 2155–2159 (1995).
32. M. Tang, R. Shekhar, and D. Huang, "Mean curvature mapping for the detection of corneal shape aberrometry," *IEEE Trans. Med. Imaging* **24**, 424–428 (2005).
33. C. Menchaca and D. Malacara, "Directional curvatures in a conic surface," *Appl. Opt.* **23**, 3258–3259 (1984).
34. A. G. Bennett, "Aspherical and continuous curve contact lenses. Part three," *Optom. Today* **28**, 238–242 (1988).
35. P. M. Kiely, G. Smith, and L. G. Carney, "The mean shape of the human cornea," *Optica Acta* **29**, 1027–1040 (1982).
36. W. F. Harris, "Curvature of ellipsoids and other surfaces," *Ophthal. Physiol. Opt.* **26**, 497–501 (2006).
37. S. Bektas, "Generalized Euler formula for curvature," *Int. J. Res. Eng. Appl. Sci.* **6**, 292–304 (2016).
38. G. W. Griffits, I. Plociniczak, and W. E. Schliesser, "Analysis of cornea curvature using radial basis functions. Part I. Methodology," *Comput. Biol. Med.* **77**, 274–284 (2016).
39. G. W. Griffits, I. Plociniczak, and W. E. Schliesser, "Analysis of cornea curvature using radial basis functions. Part II. Fitting to data set," *Comput. Biol. Med.* **77**, 285–296 (2016).
40. J. Schmit, K. Creath, and J. C. Wyant, "Surface profilers, multiple wavelength, and white light interferometry," Chapter 15 in *Optical Shop Testing*, D. Malacara, Ed., 3rd ed., pp. 667–755, Wiley, New York (2007).
41. H. I. Campbell and A. H. Greenaway, "Wavefront sensing: from historical roots to the state of the art," *EAS Publications Series* **22**, 165–185 (2006).
42. M. Lombardo and J. Lombardo, "New methods and techniques for sensing the wave aberrations of human eyes," *Clin. Exp. Optom.* **92**, 176–186 (2009).
43. D. Malacara-Hernández and Z. Malacara-Hernández, *Handbook of Optical Systems*, CRC Press, Taylor and Francis Group, Boca Raton, FL (2013).
44. D. Malacara, M. Servín, and Z. Malacara, *Interferogram Analysis for Optical Testing*, Chapters 6 and 12, 2nd Ed., Taylor and Francis, Boca Raton, FL (2005).
45. M. V. Mantravadi and D. Malacara, "Newton, Fizeau and Haidinger Interferometers," Chapter 1 in *Optical Shop Testing*, 3rd ed., D. Malacara, Ed., pp. 1–45, Wiley Interscience, New York, 2007.
46. D. Malacara, "Twyman–green interferometer," Chapter 2 in *Optical Shop Testing*, 3rd ed., D. Malacara, Ed., pp. 46–96, Wiley Interscience, New York (2007).
47. F. Twyman, "Interferometers for the experimental study of optical systems from the point of view of the wave theory," *Philos. Mag.* **35**, 49–58 (1918).
48. J. Millerd et al., "Modern approaches in phase measuring metrology," *Proc. SPIE* **5856**, 14–22 (2005).
49. J. Ojeda-Castañeda, "Foucault, wire and phase modulation tests," Chapter 8 in *Optical Shop Testing*, 3rd ed., D. Malacara, Ed., pp. 275–316, Wiley Interscience, New York (2007).
50. R. Ragazzoni et al., "Testing the pyramid wavefront sensor on the sky," *Proc. SPIE* **4007**, 423–430 (2000).

51. T. Y. Chew, R. M. Clare, and R. G. Lane, "A comparison of the Shack-Hartmann and pyramid wavefront sensors," *Opt. Commun.* **268**, 189–195 (2006).
52. S. Esposito, O. Freeney, and A. Ricardi, "Laboratory test of a pyramid wavefront sensor," *Proc. SPIE* **4007**, 416–422 (2000).
53. I. Iglesias et al., "Extended source pyramid wavefront sensor for the human eye," *Opt. Express* **10**, 419–428 (2002).
54. E. M. Daly and M. C. Dainty, "Ophthalmic wavefront measurements using a versatile pyramid sensor," *Appl. Opt.* **49**, G67–G77 (2010).
55. A. Wang et al., "Design and fabrication of a pyramid wavefront sensor," *Opt. Eng.* **49**, 73401–73405 (2010).
56. A. Cornejo-Rodriguez, "Ronchi test," Chapter 9 in *Optical Shop Testing*, 3rd ed., D. Malacara, Ed., pp. 317–360, Wiley Interscience, New York, 2007.
57. M. Strojnik, G. Paez, and M. Mantravadi, "Lateral Shear interferometers," Chapter 4 in *Optical Shop Testing*, 3rd ed., D. Malacara, Ed., pp. 122–184, Wiley Interscience, New York (2007).
58. F. Xia et al., "Highly sensitive curvature sensor based on an asymmetrical Mach-Zehnder interferometer," *Instrum. Sci. Technol.* **45**, 605–617 (2017).
59. T. Hong et al., "Method for measuring the radius of mean curvature of a spherical surface based on phase measuring deflectometry," *Appl. Opt.* **60**, 1705–1709 (2021).
60. M. Tscherning, "Die monochromatischen aberrationen des menscdhlichen Auges," *Z. Psychol. Physiol. Sinne* **6**, 456–471 (1894).
61. M. Mrochen et al., "Principles of Tscherning aberrometry," *J. Refract. Surg.* **16**, S570–S571 (2000).
62. R. Navarro and M. A. Losada, "Aberrations and relative efficiency of light pencils in the living human eye," *Optom. Vis. Sci.* **74**, 540–547 (1997).
63. J. Hartmann, "Bemerkungen uber den Bau und die Justirung von Spektrographen," *Zt. Instrumentenkd* **20**, 47–58 (1900).
64. D. Malacara-Doblado et al., "Hartmann-Shack and other screen tests," Chapter 10 in *Optical Shop Testing*, 3rd Ed., D. Malacara, Ed., pp. 361–397, Wiley Interscience, New York 2007).
65. D. Malacara-Hernández and D. Malacara-Doblado, "What is a Hartmann test," *Appl. Opt.* **54**, 2296–2301 (2015).
66. Y. Mejía-Barbosa and D. Malacara, "Object surface for applying a modified hartmann test to measure corneal topography," *Appl. Opt.* **40**, 5778–5786 (2001).
67. D. Gómez-Tejada et al., "Zonal integration of circular Hartmann and Placido patterns with non-rotationally symmetric aberrations," *J. Opt. Soc. Am. A* **37**, 1381–1384 (2020).
68. B. C. Platt and R. V. Shack, "Lenticular Hartmann screen," *Opt. Sci. Newsl* **5**, 15–16 (1971).
69. C. E. Campbell, "The range of local wavefront curvatures measurable with Shack-Hartmann wavefront sensors," *Clin. Exp. Optom.* **92**, 187–193 (2009).
70. W. Zou, K. P. Thompson, and J. P. Roland, "Differential Shack-Hartmann curvature sensor: local principal curvature measurements," *Opt. Soc. Am. A* **25**, 2331–2337 (2008).
71. I. Ghozeil and J. E. Simmons, "Screen test for large mirrors," *Appl. Opt.* **13**, 1773–1777 (1974).
72. W. H. Southwell, "Wave-front estimation from wave-front slope measurements," *J. Opt. Soc. Am.* **70**, 998–1006 (1980).
73. F. J. Gantes-Nuñez et al., "Zonal processing of Hartmann or Shack-Hartmann patterns," *Appl. Opt.* **56**, 1898–1907 (2017).
74. F. Roddier, "Curvature sensing and compensation: a new concept in adaptive optics," *Appl. Opt.* **27**, 1223–1225 (1988).
75. F. Roddier, "Wavefront sensing and the irradiance transport equation," *Appl. Opt.* **29**, 1402–1403 (1990).
76. K. Ichikawa, A. W. Lohmann, and M. Takeda, "Phase retrieval based on the irradiance transport equation and the Fourier transport method: experiments," *Appl. Opt.* **27**, 3433–3436 (1988).
77. F. Roddier and C. Roddier, "Wavefront reconstruction using iterative Fourier transforms," *Appl. Opt.* **30**, 1325–1327 (1991).

78. C. Paterson and J. C. Dainty, "Hybrid curvature and gradient wave-front sensor," *Opt. Lett.* **25**, 1687–1689 (2000).
79. J. Nam, L. N. Thibos, and D. R. Iskander, "Describing ocular aberrations with wavefront vergence maps," *Clin. Exp. Optom.* **92**, 194–205 (2009).
80. M. Corbet et al., *Corneal Topography, Principles and Applications*, 2nd Ed., Chapter 5, Springer, Switzerland AG (1998).
81. J. Hernández-Delgado et al., "Curvature or power maps of an optical surface or a wavefront," *Opt. Commun.* **495**, 127083 (2021).

Zacarías Malacara-Hernández holds a position as researcher at Centro de Investigaciones en Óptica in León México for 40 years. He currently works in optical instrumentation and optical testing. He is involved in teaching and the study of optical surfaces and wavefront description.

Biographies of the other authors are not available.